Instituto de Neurociencias
Consejo Superior de Investigaciones Científicas
Universidad Miguel Hernández

Prrx1 FACTOR CONTROLS ORGAN POSITIONING IN VERTEBRATES

Doctoral Thesis
Hakan Coşkun

Supervisor
M. Ángela Nieto

San Juan de Alicante, 2017

Instituto de Neurociencias
Consejo Superior de Investigaciones Científicas
Universidad Miguel Hernández

Prrx1 FACTOR CONTROLS ORGAN POSITIONING IN VERTEBRATES

DOCTORAL THESIS
HAKAN COŞKUN

Supervisor:
M. ÁNGELA NIETO

San Juan de Alicante, 2017

Dr. Salvador Martínez Pérez, Director del Instituto de Neurociencias, centro mixto UMH-CSIC,

CERTIFICA que la tesis doctoral titulada “Prrx1 Factor Controls Organ Positioning in Vertebrates”, ha sido realizada por D. Hakan Coşkun, bajo la dirección de la Dra. M. Ángela Nieto y da su conformidad para que sea presentada a la Comisión de Doctorado de la Universidad Miguel Hernández.

Para que así conste a los efectos oportunos, firmo el presente certificado en San Juan de Alicante a 19 de Septiembre de 2017.

Fdo.: Prof. Salvador Martínez Pérez
Director del Instituto de Neurociencias

La Dra. M. Ángela Nieto, Profesora de Investigación del Consejo Superior de Investigaciones Científicas en el Instituto de Neurociencias, centro mixto CSIC-UMH,

DA SU CONFORMIDAD a la lectura de la tesis doctoral titulada "Prrx1 Factor Controls Organ Positioning in Vertebrates", realizada por D. Hakan Coşkun, bajo mi inmediata dirección y supervisión en el Instituto de Neurociencias (CSIC-UMH) y que presenta para la obtención del grado de Doctor por la Universidad Miguel Hernández.

Para que así conste a los efectos oportunos, firmo el presente certificado en San Juan de Alicante a 19 de Septiembre de 2017.

Fdo.: Dra. M. Ángela Nieto Toledano

To my parents, Melek and Muzaffer,

Thanks for your great support!

ACKNOWLEDGEMENTS

I would like to thank to my PhD supervisor, Prof. M. Angela Nieto for supporting me during these past five years. Yes, it is five years. I met with her for the first time when I was reading her articles during my master education. Then, she kindly accepted and hosted me in her lab for summer internship and my PhD adventure has been started. Finally, I am writing my PhD thesis, now. The door to Prof. Nieto office was always open whenever I ran into a trouble spot or had a question about my research. I am grateful to her for giving me the great opportunity of working and carrying out the doctoral thesis in her lab; I wouldn't be where I am now and I wouldn't have learned as much without this opportunity.

I would also like to thank to Oscar Ocaña who was involved teaching and helping me in this research project. I think that we did a great job together and finally we reap the fruits of our hard work. When we were working in the lab until 4 am, I was sure that we will succeed.

I wish to acknowledge the support of my colleagues: Joan Galcerán Saez, Berta López Sánchez-Laorden, Aida Arcas Mantas, Khalil Kass Youssef, Luciano Francisco Rago, Sonia Vega de los Reyes, Verona Villar Cerviño, Ainara González Iglesias, Francisco García Asencio, Hassan Fazilaty, Noemí Castroviejo Jiménez, Sebastián Martínez López, Sergio Cano Peiró who have always been of great help and who were great companion and source of knowledge and experience. I am grateful for the assistance of technician and administration staff in the lab: Cristina López Blau, Diana Abad Bataller, Sandra Moreno Valverde and Auxi Casanova Javaloyes. They were always very kind, helpful and understanding.

I am grateful to my parents Melek Coşkun and Muzaffer Coşkun and my dear brother Murat Coşkun, who have provided me through moral and emotional support in my life. I am also grateful to my other family members and friends who have supported me along the way. Special thanks to Birol Ay, Ali Ulucan, Merve Kutlu and Velaria Pecoraro.

A very special gratitude to Santiago Grisolía Fellowship Programme from the Valencian Ministry of Education for providing the bursary for my PhD thesis.

ABBREVIATIONS

- A: atrium
- AIP: anterior intestinal portal
- CF: cardiac folds
- C: coelom
- DSpLM: dorsal splanchnic lateral mesoderm
- E: eyes
- EC: ectoderm
- FG: foregut
- HT: heart tube
- IFT: inflow tract
- LPM: lateral plate mesoderm
- LSH: left *sinus venosus* horn
- LVV: left vitelline vein
- NC: neural crest
- N: notochord
- NP: neural plate
- NT: neural tube
- OFT: outflow tract
- P: pericardium
- PHT: primary heart tube
- PLPM: posterior lateral plate mesoderm
- PP: posterior pole
- PV: pericardial vesicle
- RSH: right sinus venosus horn
- RVV: right vitelline vein
- S: somite
- SHF: secondary heart field
- SH: sinus venosus horns
- SoLM: somatic lateral mesoderm
- SpLM: splanchnic lateral mesoderm
- SV: sinus venosus
- V: ventricle
- VP: venous pole
- VSpLM: ventral splanchnic lateral mesoderm
- VV: vitelline veins
- YS: yolk sac

SUMMARY

The majority of animals exhibit an external bilateral symmetry. However, there are numerous internal left–right (L/R) asymmetries, including the morphology and position of several organs. During development, all these asymmetries are established by complex genetic and epigenetic cascades.

In vertebrates, left identity is mediated by the TGFβ family member Nodal and its downstream target Pitx2, being both transiently expressed in the left lateral plate mesoderm (LPM). This left-handed information is repressed on the right-hand side by the epithelial-mesenchymal transition (EMT) inducer Snail1. So far, it has been unclear whether an equivalent right-handed pathway is providing instructive information to the right LPM.

Recently in our lab, we have identified a right-handed pathway that drives heart looping in zebrafish. This novel pathway is regulated by a BMP-mediated asymmetric L/R activation of Prrx1a, another EMT inducer, in the LPM. Prrx1a is transiently expressed at higher levels on the right-hand side of the embryo, and its downregulation prevents heart looping and leads to mesocardia. Prrx1a drives differential cell movements leading to a leftward displacement of the cardiac posterior pole that promotes dextral looping through an actomyosin-dependent mechanism. Thus, two parallel and mutually repressed pathways exist in the left and right LPM. Activation of Nodal (on the left) and BMP (on the right) converge on the asymmetric activation of two paired-like homeodomain transcription factors, Pitx2 and Prrx1, respectively. As the left cascade has been involved in heart morphogenesis, the integration of both pathways would ultimately govern heart morphogenesis and laterality.

In this thesis project, we expanded our study to understand whether this L/R asymmetric signalling pathway is conserved during evolution. Indeed, transient asymmetric distribution of Prrx1 is also evident in the chick LPM, with higher levels on the right-hand side, and downregulation of Prrx1 in the chick embryo also induces mesocardia. The asymmetric L/R Prrx1 expression in the chick is also compatible with the formation of an actomyosin- dependent mechanism. As in the fish, Prrx1 silencing caused a loss of actin fibers and of L/R morphological asymmetry. We find that this mechanism is also conserved in the mouse, where Snail1 fulfils the role of Prrx1 in the fish and chick. Furthermore, we next analysed whether Prrx1 was also important for

asymmetric positioning of other organs. Here we show that downregulation of Prrx1a also affects gut looping and impairs the asymmetric positioning of gut, liver and pancreas in zebrafish, leading to embryos in which both the heart and the endodermal organs are kept in the midline.

Thus, we propose that a right-handed differential L/R EMT produces asymmetric forces and drives organ laterality in vertebrates.

Published paper related to this thesis:

Oscar H. Ocaña, Hakan Coskun, Carolina Minguillón, Prayag Murawala, Elly M. Tanaka, Joan Galcerán, Ramón Muñoz-Chapuli and M. Angela Nieto, A right-handed signalling pathway drives heart looping in vertebrates. Nature, DOI 10.1038/nature23454, in press.

RESUMEN

La mayoría de los animales muestran una simetría bilateral externa. Sin embargo, hay numerosas asimetrías internas (L/R del inglés; izquierda, Left y derecha, Right) incluyendo la morfología y posición de varios órganos. Durante el desarrollo embrıonario, todas las asimetrías se establecen mediante cascadas genéticas y epigenéticas complejas.

En los vertebrados, la identidad izquierda esta mediada por Nodal, un miembro de la familia TGFβ y su gen diana *Pitx2*. Ambos se expresan transitoriamente en el mesodermo lateral izquierdo (LPM). Esta información izquierda se reprime en el lado derecho por el inductor de la transición epitelio-mesénquima (EMT) Snail1. Hasta ahora, no se conocía si existía una vía de señalización equivalente que proporcionase información instructiva también en el LPM derecho.

Recientemente, hemos identificado en nuestro laboratorio una vía de señalización derecha que regula la posición del corazón en el pez cebra. Esta nueva vía está mediada por la activación asimétrica (L/R) de otro inductor de EMT (Prrx1a) mediada por BMP. Prrx1a se expresa transitoriamente de manera asimétrica, con niveles más elevados en el lado derecho del embrión, y su represión impide el giro del corazón e induce mesocardia. Prrx1a dirige movimientos celulares diferenciales que llevan a un desplazamiento hacia la izquierda del polo cardiaco posterior, lo cual promueve un giro dextrógiro por un mecanismo dependiente de actomiosina. Por tanto, existen dos vías de señalización paralelas y mutuamente reprimidas en los mesodermos laterales (LPM) izquierdo y derecho. La señalización de Nodal (en la izquierda) y de BMP (mayor a la derecha) converge en una activación asimétrica de dos factores de transcripción que contienen el dominio “paired-like”, Pitx2 y Prrx1, respectivamente. Como la cascada de señalización izquierda se ha involucrado en la morfogénesis del corazón, la integración de ambas vías gobierna la morfogénesis y la lateralidad del corazón.

En este proyecto de Tesis hemos expandido nuestro estudio para entender si estas vías de señalización asimétricas L/R se han conservado en la evolución. De hecho, la distribución asimétrica de Prrx1 se conserva en el LPM del embrión de pollo con unos niveles más altos en el lado derecho, y la bajada de la expresión de Prrx1 en el pollo también induce mesocardia. La función de Prrx1 en el pollo es también compatible con un mecanismo dirigido por actomiosina. Como en el pez, el

silenciamiento de Prrx1 causa una pérdida de fibras de actina y de la asimetría L/R. Hemos encontrado que este mecanismo se conserva también en el ratón donde Snail1 realiza el papel de Prrx1 en el pez y en el pollo. Además, hemos analizado si Prrx1 es también importante para el posicionamiento asimétrico de otros órganos. Mostramos que la reducción de la expresión de Prrx1a también afecta el giro normal del intestino y afecta la posición asimétrica del intestino, el hígado y el páncreas en el pez cebra, produciendo animales en los que tanto el corazón como los órganos endodérmicos permanecen en la línea media.

Por tanto, proponemos que una transición epitelio-mesénquima diferencial, más prominente en el lado derecho produce fuerzas asimétricas que regulan la lateralidad de los órganos en los vertebrados.

Publicaciones relacionadas con la tesis:

Oscar H. Ocaña, Hakan Coskun, Carolina Minguillón, Prayag Murawala, Elly M. Tanaka, Joan Galcerán, Ramón Muñoz-Chapuli and M. Angela Nieto, A right-handed signalling pathway drives heart looping in vertebrates. Nature, DOI 10.1038/nature23454, in press.

INDEX

I. INTRODUCTION

I.1 Left-Right Internal Organ Asymmetry in Vertebrates

The external body plan of most metazoans exhibits bilateral symmetry. This symmetry is illustrated by Leonardo da Vinci's description of the "Vitruvian Man" that describes some of the uniform proportions of the human body (Figure 1). However, various internal organs display asymmetric positioning and/or orientation in the left-right (L/R) axis, including the heart, liver or pancreas in vertebrates. During organogenesis, the primordia of the unpaired organs of the chest and abdomen first appear in the midline and then lateralize. In vertebrates, the first morphological marker of L/R asymmetry is the right-sided looping of the developing heart. A second sign of asymmetry is then manifested by the rotation of the body in vertebrates. Finally, all internal organs show L/R asymmetry (Raya and Izpisua Belmonte 2006).

The L/R asymmetries of internal organs are similar in different species and have been conserved throughout evolution (Speder et al. 2007). L/R defects in humans are phenotypically variable and genetically heterogeneous. The normal asymmetric arrangement of the organs is called *situs solitus* and occurs in 99% of humans. However, clinically significant laterality defects arise in around 1/10,000 births (A. E. Lin et al. 2014). Thus, we need to better understand the establishment of organ laterality during embryogenesis and therefore, it is important to identify genes and mechanisms that are involved in organ positioning.

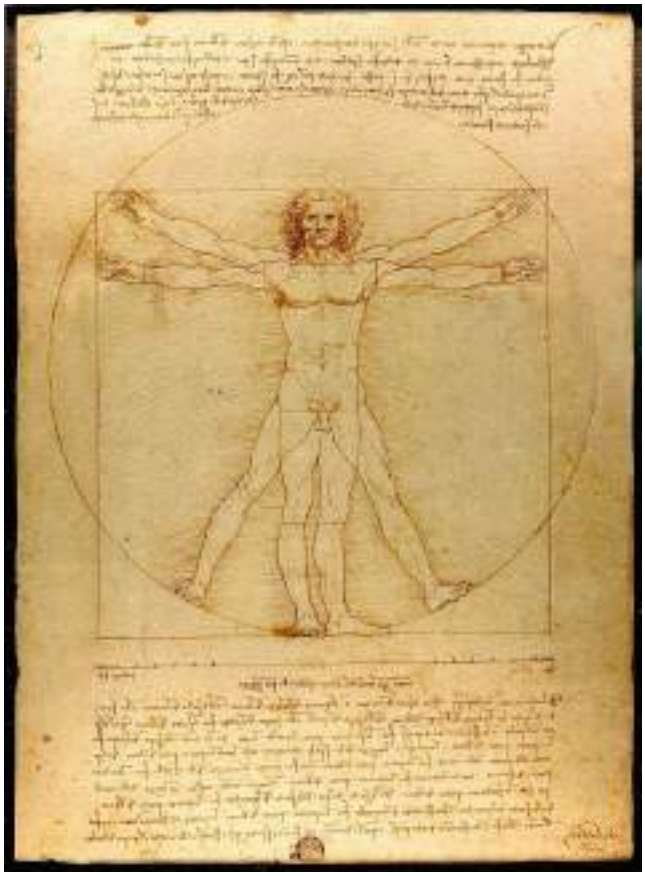

Figure 1. The bilateral symmetry of human body. Animals that are bilaterally symmetric have mirror symmetry in the sagittal plane, which divides the body vertically into left and right halves, with one of each sense organ and limb pair on either side. *"Vitruvian Man" 1490, Leonardo da Vinci*

I.1.1 Breaking the Bilateral Symmetry of the Embryo

The establishment of L/R asymmetry in vertebrates involves multiple cellular and molecular processes. During gastrulation, the primitive streak extends through the midline and the anteroposterior body axis. The most anterior portion of the primitive streak, which is called the primitive pit, becomes the embryonic node in the mouse. The node receives different names in chick (Hensen's node) or zebrafish (Kupffer's vesicle) (Davidson and Tam 2000; Essner et al. 2005). Thus, the first L/R symmetry breaking leads to a leftward flow of Nodal at the node (Okada et al. 2005) generated by the clockwise rotation of cilia and the participation of non-motile cilia (Hirokawa et al. 2006; Hirokawa et al. 2009; Speder et al. 2007). During nodal flow, nodal vesicular parcels (NVPs) are transported to the left. This event is stimulated by FGFR (fibroblast

growth factor receptors) signalling (Figure 2). The Nodal flow is conserved between fish, mice and rabbit.

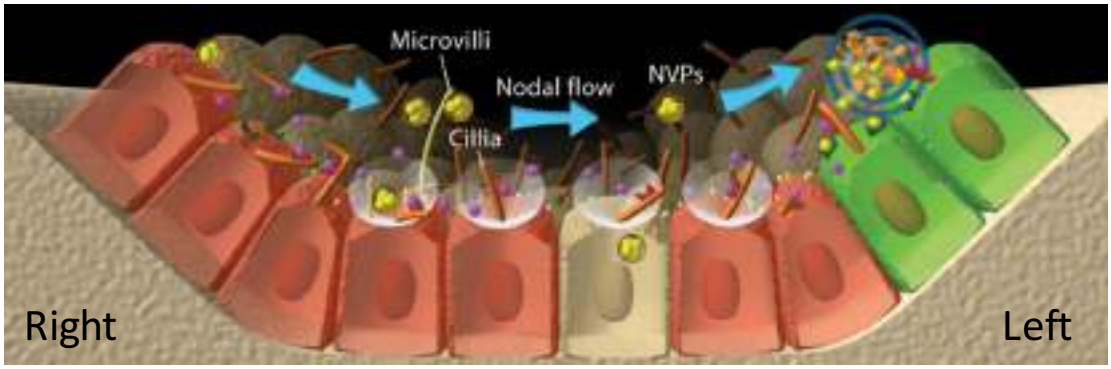

Figure 2. The nodal flow. Motile monocilia at the embryonic node generate a leftward flow of extra-embryonic fluid by their circular movements. The nodal vesicular parcels (NVPs) are secreted from the right side of the embryonic node and transported to the left side by the nodal flow. This event is stimulated by FGFR signalling (Purple) (Adapted from *Hirokawa et al.*, 2006).

I.1.2 Molecular Pathways in Left-Right Asymmetry

After establishing L/R identity around the node, it is essential to transfer this information to the LPM at early somitogenesis stages, as most of the organs that display L/R asymmetries are derived from the LPM. However, this phenomenon is still not fully understood. The discovery of asymmetric gene expression patterns in chick embryos opened the field more than 2 decades ago. Some of these key players are Nodal, Lefty1 and Lefty2, Pitx2 (Paired-like homeodomain transcription factor 2), Bmp4 (Bone morphogenetic protein 4), Shh (Sonic hedgehog) and Fgf8 (Fibroblast growth factor 8) (Raya and Izpisua Belmonte 2006) (Figure 3). During the early stages of L/R determination, chick embryos express Shh on the left side of the node and its expression is necessary and sufficient to induce Nodal expression in the left LPM (Levin et al. 1995; Logan et al. 1998). Bmp4 signalling is also necessary and sufficient to maintain Shh asymmetry within the node. Shh and Bmp4 proteins negatively regulate each other's transcription, resulting in a strict complementary gene expression pattern at both sides of the node (Monsoro-Burq and Le Douarin 2001).

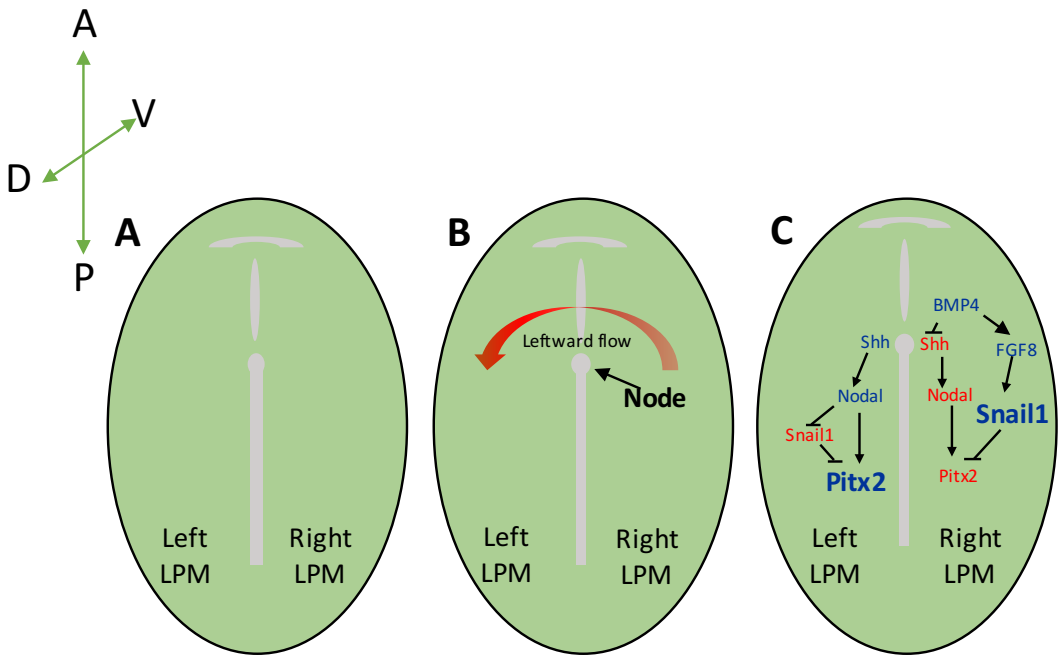

Figure 3. Early left–right asymmetrical genetic cascades in vertebrates. (**A**) Initial breaking of bilateral symmetry that generates left-right information, although the nature is unknown or not applicable to some organisms. (**B**) The L/R information is transmitted to the node, which generates a leftward flow through their cilia, giving rise to local asymmetries. (**C**) These asymmetries around the node are conveyed to the lateral plate mesoderm (LPM). Nodal and its downstream target Pitx2 are expressed in the left LPM, while Snail1 is expressed higher levels in the right LPM, where it represses left-handed information. A, anterior; P, posterior; D, dorsal; V, ventral.

I.1.2.1 Nodal

Nodal is a member of TGF- β family and it is conserved in deuterostomes and protostomes (Chea et al. 2005). The asymmetric initiation of Nodal around the node plays a central role in subsequent organization of left-right axial structures (Dougan et al. 2003; Shen 2007). Nodal signalling plays a crucial role in signal transfer from the node to LPM (Branford and Yost 2004; Kawasumi et al. 2011) resulting in the asymmetric expression of its downstream targets, including Lefty 1 and 2, and Pitx2 (Patel et al. 1999; Soukup et al. 2015; Wright 2001). While Nodal and Pitx2 are expressed in the left LMP, Nodal expression is repressed by Bmp4 on the right side (Raya and Izpisua Belmonte 2006), leading to a leftward restriction in the LPM that controls L/R internal organ positioning (Raya and Izpisua Belmonte 2006). Nodal is

also involved in cell differentiation at gastrulation stages and required to establish the anterior-posterior axis (Brennan et al. 2001).

I.1.2.2 Paired like homeodomain transcription factor 2: Pitx2

Pitx2 is a member of the Pitx/RIEG family of homeobox-containing genes. The homeodomain is related to that of the *Drosophila paired* gene, and the protein also contains an OAR transactivation domain (Semina et al. 1997). It is expressed in anterior mesoderm and the left LPM in mouse, chick, *Xenopus* and zebrafish, as is a direct target of Nodal, as mentioned above (Campione et al. 1999; Logan et al. 1998; Ryan et al. 1998). In addition, Pitx2 is expressed in the developing eye (Semina et al. 1996) and in the tooth primordia (Mucchielli et al. 1997) during embryogenesis, and it plays a key role in embryonic and adult myogenesis (Hernandez-Torres et al. 2017).

Pitx2 is best known for its important role in the establishment of the left-right asymmetries of internal organs (Ryan et al. 1998). Its three isoforms, *Pitx2a*, *Pitx2b* and *Pitx2c*, display different expression patterns and regulation, and have different functions during asymmetric organ development (Essner et al. 2000). However, only Pitx2c plays a crucial role in left-right axis determination and was described to be involved in heart laterality (Schweickert et al. 2000; Yu et al. 2001) and gut looping in chicken and mouse embryos (N. M. Davis et al. 2008; Kurpios et al. 2008). However, *Pitx2* mouse mutants do not display heart looping defects but rather, they develop cardiac right isomerism – the absence of a left-hand side and the presence of a mirror image duplication of right-hand morphological features (Campione et al. 1999; C. R. Lin et al. 1999). Furthermore, recent data show that *Pitx2* mutations do not affect either heart or gut looping in zebrafish (Ji et al, 2016). Interestingly, recent data from our lab indicate that heart looping is mediated by a L/R symmetric EMT, more prominent from the right (Ocana et al. 2017).

The mechanism by which Pitx2 confers left identity to internal organs is still unknown. Therefore, identifying its downstream targets is crucial to understand this process.

I.1.2.3 Bone Morphogenetic Protein 4: Bmp4

Bone Morphogenetic Proteins (BMPs) are members of the TGFß superfamily. BMPs play critical roles during early vertebrate development (Wang et al. 2014), including mesoderm formation and cardiac development. As such, loss of Bmp2 or Bmp4 results in embryonic lethality and Bmp1, Bmp7, and Bmp11 knockout mice die shortly after birth (Wang et al. 2014).

Bmp4, in addition to regulate cartilage and bone development, can also induce the epithelial to mesenchymal transition (EMT) (Kestens et al. 2016; Theriault et al. 2007) and has also been implicated in the regulation of L/R patterning during early embryogenesis (Monsoro-Burq and Le Douarin 2001; Ramsdell and Yost 1999). The right-sided expression of Bmp4 is initiated by an activin-like activity. Thus, activin upregulates Bmp4 on the right LMP that in turn, upregulates Fgf8 expression, which induces Snail1 expression (Boettger et al. 1999; Shen 2007). On the other hand, Bmp4 represses Nodal in the right LPM (Smith et al. 2011), contributing to the asymmetric organisation of the internal organs.

I.2 Asymmetric Positioning of the Internal Organs in Embryonic Development

I.2.1 Establishment of Cardiac Laterality

In the initial stages of development, the embryo appears symmetrical with respect to the midline. The first clear evidence of morphological asymmetry is the looping of the heart (Icardo et al. 2002). Conceptually, establishment of cardiac laterality takes place in four different phases. During early embryonic development, two endocardial tubes fuse on the midline and form a straight heart tube (Figure 4A). Then, L/R differential cell movements towards the midline lead to a leftward displacement of the cardiac posterior pole (Ocana et al. 2017) and the heart tube loops toward the right side (Figure 4B) The leftward torsion deforms the looping tube into a helically coiled loop which is called C-shaped loop (Figure 4C). Then, the loop acquires the complex helical configuration and gains a S-shaped form (Figure 4D). Finally, the heart develops on the left side. If the heart tube had looped toward the left side instead of the right side, the final position of the heart would be on the right side. This condition is called

dextrocardia and although pathological, it is still compatible with life (Figure 4E). However, mesocardia, the condition in which the heart does not loop and develops in the midline, it is not life compatible (Icardo et al. 2002).

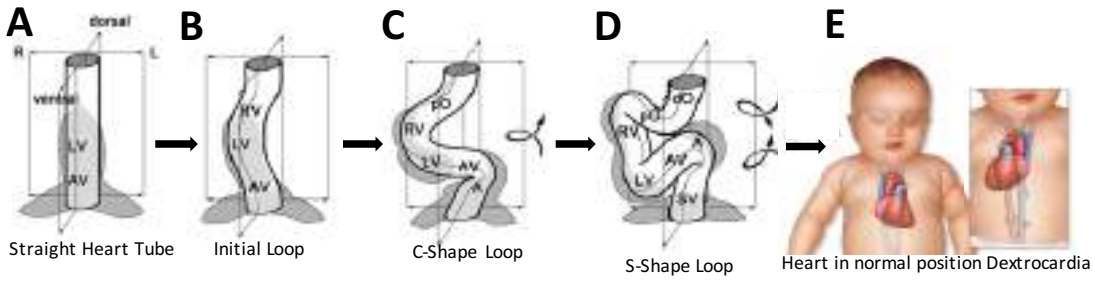

Figure 4. Establishment of cardiac laterality. (**A**) Formation of primitive heart tube in the midline. (**B**) Initial looping of the heart tube toward to right side. (**C**) The heart loops helically coiled and gains the C-shape form. (**D**) The heart looping acquires the complex helical configuration and gains S-shaped form. (**E**) The final position of the heart. The heart develops on the left side as a normal position. Note that the mirror image of the normal position of the heart, Dextrocardia, with the heart located on the right side of the body. A, atrium; AV, atrio-ventricular canal; LV, left ventricle; dO, distal outflow tract; pO, proximal outflow tract; RV, right ventricle; SV, *sinus venosus*. (Adapted from *Bayraktar et.al, 2014* and *A.D.A.M.* images)

The key steps of heart development in zebrafish are similar to those in human and other mammals. Basically, differentiated cardiac precursors form a heart tube, and then the heart tube loops and builds an atrial and ventricular chamber separated by an atrio-ventricular (AV) valve (Bakkers 2011). The process starts at gastrulation, when cardiac progenitor cells migrate towards the embryonic midline to from the cardiac disc (Figure 5A). The cells continue to fuse at midline at about 18 hpf (Figure 5B). After cardiac fusion, an elongated form develops which is called the cardiac cone (Figure 5C). The cardiac cone expands and shifts from midline towards the left side, through a process known as cardiac jogging. After jogging, the heart tube elongates (cardiac extension) and a leftward displacement of the cardiac posterior pole promotes a subsequent dextral looping to create an S-shaped form (cardiac looping*)* (Figure 5D). The AV canal becomes detectable and the endocardial cells form the endocardial cushions (Figure 5E).

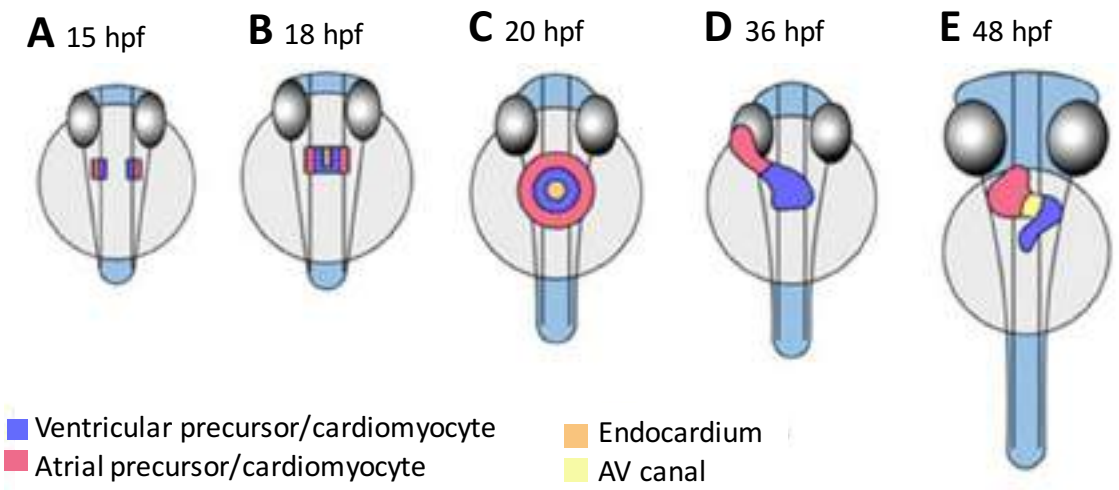

Figure 5. Stages of heart formation in zebrafish embryos in a ventral view. (**A**) Cardiac precursors move towards the anterior LPM. The atrial precursors are located laterally, the ventricular precursors medially at 15 hpf. (**B**) Cardiac fusion starts at about 18 hpf at the posterior end of the bilateral heart fields. Endocardial cells arrive first at midline, followed by ventricular cells. The atrial precursors do so slightly later, and the structure formed is called cardiac disc. (**C**) After cardiac fusion the cells form the cardiac cone. The cardiac cone starts to transform into the heart tube by 21 hpf. (**D**) Cardiac looping of the heart tube occurs between 26 hpf and 48 hpf. The linear heart tube bends and creates an S-shaped loop. By 36 hpf the atrium and ventricle become distinguishable. (**E**) The heart tube rotates. The AV canal develops by constriction of the boundary between atrium and ventricle. hpf: hours post fertilisation, AV: atrioventricular canal (Adapted from *Keßler et al*., 2012)

I.2.2 Laterality of Endodermal Organs

The endodermal organs also display L/R asymmetric positioning. During embryonic development, the gut tube develops at the midline and then proper looping of intestine in the abdominal cavity results in the asymmetrical positioning of liver, pancreas, lungs and gut (Horne-Badovinac et al. 2003). Endoderm derived organs are surrounded by mesoderm, and the interaction between these two tissues is critical for organogenesis (Cayuso et al. 2016; A. Davis et al. 2017). Thus, the epithelial LPM determines the chirality of gut looping and the final position of endodermal organs in the fish (Yin et al. 2010) and also in amniotes (N. M. Davis et al. 2008; Kurpios et al. 2008).

Gut looping in zebrafish is under control of left and right LPM. The first leftward bend of the developing intestine takes place between 26-30 hpf (Figure 6). At 24 hpf, the left and right LMP have a U-shaped structure composed of two rows of epithelial cells. From 24 to 26 hpf, the left and right LPM fuse in the midline and undergo an asymmetric L/R migration as shown in Fig. 6, either dorsally or ventrally toward the embryonic midline in a way that the right LPM pushes the gut leftwards with respect to the midline. These LPM movements have been proven to be autonomous and under the control of Nodal signalling (Horne-Badovinac, 2003; Yin et al. 2010).

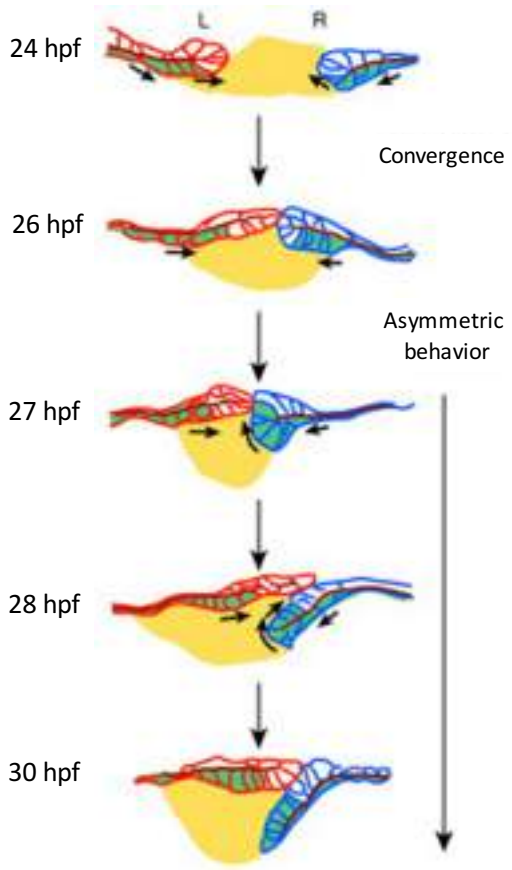

Figure 6. Asymmetric migration of LPM during gut looping in zebrafish. 24 hpf, the left and right LPM are located lateral to the gut. Each side has a U-shaped structure composed of two rows of epithelial cells. The ventral half expresses *hand2*, which can be observed with a *hand2:eGFP* transgenic line. From 24 to 26 hpf, the left and right LPM converge in the midline after migrating on top of the gut. Between 26 and 30 hpf, the LPM undergoes asymmetric migration: whereas the right LPM moves ventrolateral to the gut, the left LPM migrates dorsally. The gut is yellow, the left LPM is red, the right LPM is blue, and the *hand2:eGFP* expressing cells are green. The dark red line represents the apical side of the LPM epithelium. Arrows indicate the direction of migration of the *hand2*:*eGFP* expressing cells (Adapted from *Yin et. al*., 2010).

The chirality of midgut looping in mammals and birds is determined by the L/R asymmetrical architecture of the dorsal mesentery (DM) (Davis et al., 2008; Hecksher-Sorensen et al., 2004; Kurpios et al., 2008). DM is a structure that surrounds the primitive gut tube and connects the gut tube with the dorsal body wall. The embryonic DM consists of four cellular compartments: left and right epithelium and mesenchyme (Figure 7). During gut rotation, the position of DM cellular compartments is modified (Welsh et al. 2013). In the chicken, DM forms on day 3 (Hamburger-Hamilton [HH] stage 19) (Hamburger and Hamilton, 1992), in an initially bilateral symmetric manner. However, DM cells reorganize through epithelial shape changes also involving mesenchymal condensation (left) or expansion (right) within 10–12 hours (HH21) (Figure 7). While the left epithelium preserves its columnar shape, the right epithelium gains cuboidal morphology, and the left mesenchyme aggregates whereas the right mesenchyme disperses. Consequently, the left DM shortens while the right side lengthens relative to the dorsal-ventral (D-V) axis. Deformation of the DM shifts the gut tube to the left. This structural change is accompanied by changes in the extracellular matrix (ECM) and cell-cell adhesion molecules, and the process is controlled by the transcription factors Pitx2 and Isl1, specifically expressed on the left side, and Tbx18, specifically expressed on the right side (N. M. Davis et al. 2008).

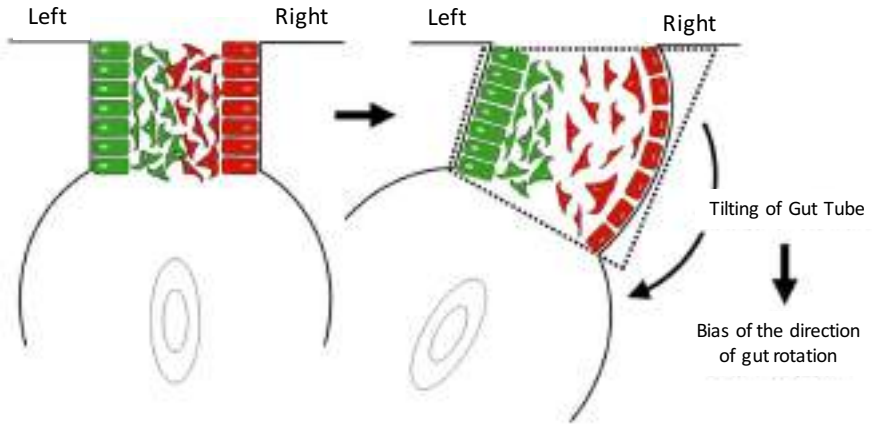

Figure 7. The directional looping of the gut tube in amniotes. The chirality of gut looping is determined by left-right asymmetries in the cellular architecture of the dorsal mesentery, the structure that connects the primitive gut tube with the body wall. The mesenchymal cells of the dorsal mesentery are more condensed on the left (green) than on the right side (red). The overlying epithelium on the left side exhibits a columnar morphology, in contrast to a cuboidal morphology on the right side (Adapted from *Davis et. al.,* 2008).

I.3 The Concept of Epithelial Plasticity: Epithelial-Mesenchymal Transition

Epithelial to Mesenchymal Transition (EMT) is a process by which epithelial cells lose their apico-basal polarity and intercellular adhesion complexes, and gain migratory and invasive properties to become mesenchymal cells. The reverse of this process -mesenchymal to epithelial transition (MET)- is associated with the loss of migration and with cells reacquiring apico-basal polarization and junctional complexes, the hallmarks of epithelial tissues (Kalluri and Weinberg 2009; Thiery et al. 2009). The EMT plays crucial roles in the formation of the body plan and in the differentiation of multiple tissues and organs. The reactivation of EMT programmes in the adult is key for the development of fibrosis, for wound healing and for the delamination of cells from the primary tumour (Figure 8) (Grande et al. 2015; Lovisa et al. 2015; Nieto et al. 2016).

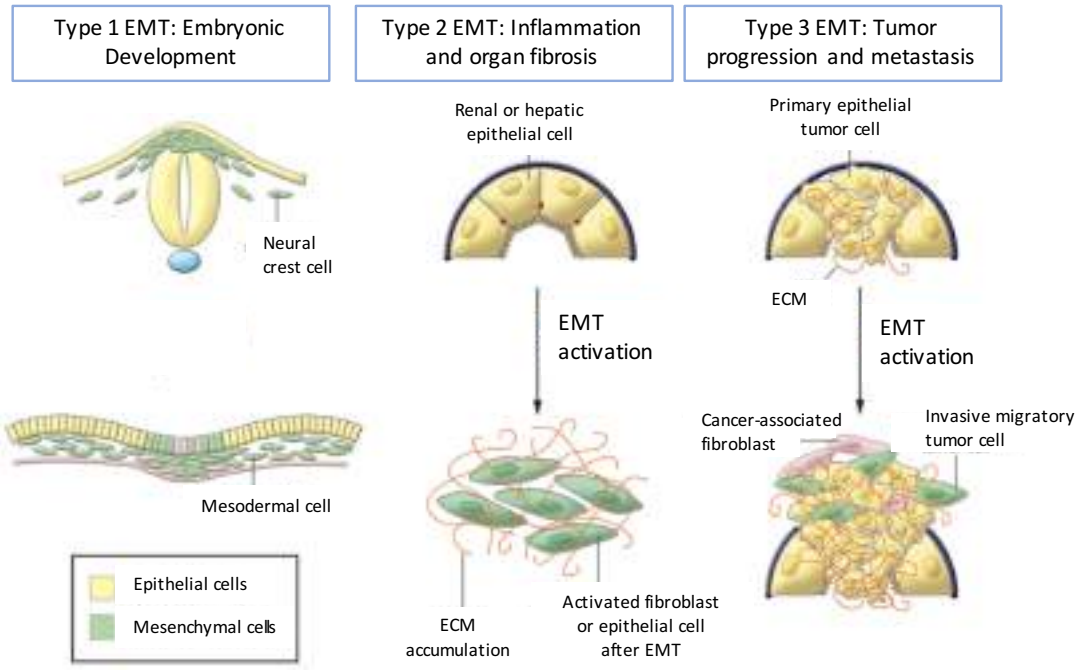

Figure 8. Different types of EMT. Type 1 EMT is associated with neural crest cells delamination and embryonic gastrulation. Type 2 EMT occurs in the context of inflammation and fibrosis. Unlike type 1 EMT, type 2 EMT takes place over extended periods of time and can destroy an affected organ if the primary inflammatory insult is not removed. Type 3 EMT is associated with cancer progression (Adapted from *Acloque et. al*., 2009 and *Kalluri and Weinberg*, 2009).

The transition from the epithelial to the mesenchymal phenotype includes a spectrum of inter- and intracellular changes. These chances are determined by the integration of extracellular signals the cell receives (Nieto et al. 2016). The EMT process occurs into several steps (Figure 9). It is still not clear whether the EMT can be considered as a continuum, whereby cells exhibit epithelial (E), intermediate (EM), and mesenchymal (M) phenotypes, or whether intermediate discrete metastable states exist. Evidence for the latter can be found in different contexts including the reactivation of EMT during renal fibrosis (Grande et al. 2015). The intermediate phenotypes are the result of the activation of a partial EMT programme.

The EMT can be induced by different signals (e.g., hypoxia, growth factors, etc.), and cells pass through a thermodynamic hump that leads to different phenotypes (e.g., EM1; EM3) (Nieto et al. 2016). This signal converges in the activation of transcription factors called EMT-TFs (including Snail, Zeb, Twist and Prrx families), post-transcriptional regulators (miRNAs) and the epigenetic control at the promoters of relevant genes (Nieto et al. 2016).

The structural changes behind the EMT can be described as follows:

1- Disruption of the intercellular adhesion complexes and loss of apico-basal polarity: Cells sequentially lose apico-basal polarity and cell-cell adhesion complexes, including tight junctions, adherens junctions, desmosomes and gap junctions.

2. Profound cytoskeletal remodelling: The cells gain front-back polarity and enhance cell matrix interactions.

3. Activation of mesenchymal markers and of invasive properties

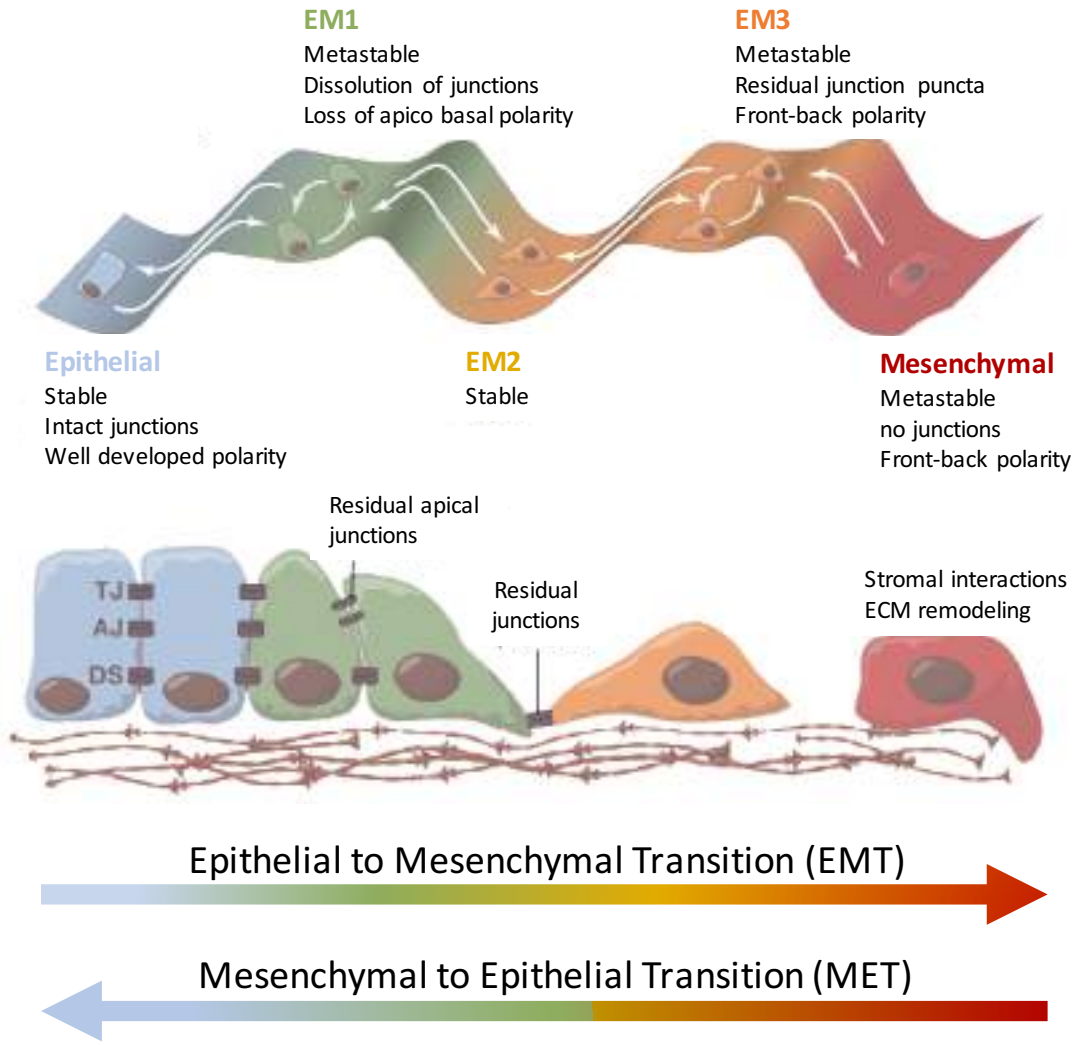

Figure 9. Epithelial to mesenchymal transition (EMT) spectrum through the different states. Cells can exhibit epithelial (E), intermediate (EM), and mesenchymal (M) phenotypes during EMT. First, they lose apico-basal polarity and cell-cell adhesions and then they gain front-back polarity and enhanced cell matrix interactions. The coloured spectrum denotes hypothetical transitions. When the system is perturbed in response to EMT signals, cells could pass through a thermodynamic hump that leads to a distinct phenotype (e.g., EM1; EM3). The backward arrows represent the reversal to more epithelial states. The existence of quasi-stable transitional states is also predicted and found in different contexts (e.g., EM2). TJ, tight junction; AJ, adherens junction; DS, desmosome (Adapted from *Nieto et. al*., 2016).

I.3.1 Epithelial-Mesenchymal Transition During Embryonic Development

Throughout evolution, the capacity of a cell to transition from an epithelial to a mesenchymal state has been fundamental in the generation of complex body patterns (Acloque et al. 2009). Several rounds of the EMT and MET are necessary in the embryo for the final differentiation of specialized cell types and the acquisition of complex three-dimensional structure of internal organs (Thiery et al. 2009). Indeed, all adult tissues and organs are the result of one or several rounds of EMT and MET with the exception of the epidermis and the anterior central nervous system (Figure 10).

Primary EMT occurs at gastrulation and during delamination of neural crest cells, both fundamental during embryonic development (Acloque et al. 2009). Primary EMTs are followed by differentiation steps that generate different cell types, which often involve the reverse MET process. Early mesodermal cells are subdivided into axial, paraxial, intermediate, and lateral mesoderms that then transiently pass through epithelial states to form the notochord, the somites, and the somatopleure and splanchnopleure. These transient structures undergo secondary EMTs, generating mesenchymal cells that later differentiate into specific cell types. The cardiac valve progenitor cells are the result of a tertiary EMT, undergone by endocardial cushions (von Gise and Pu 2012). Moreover, the epicardium also undergoes EMT to generate vascular cells and myofibroblasts (E. Cano et al. 2016; Krainock et al. 2016).

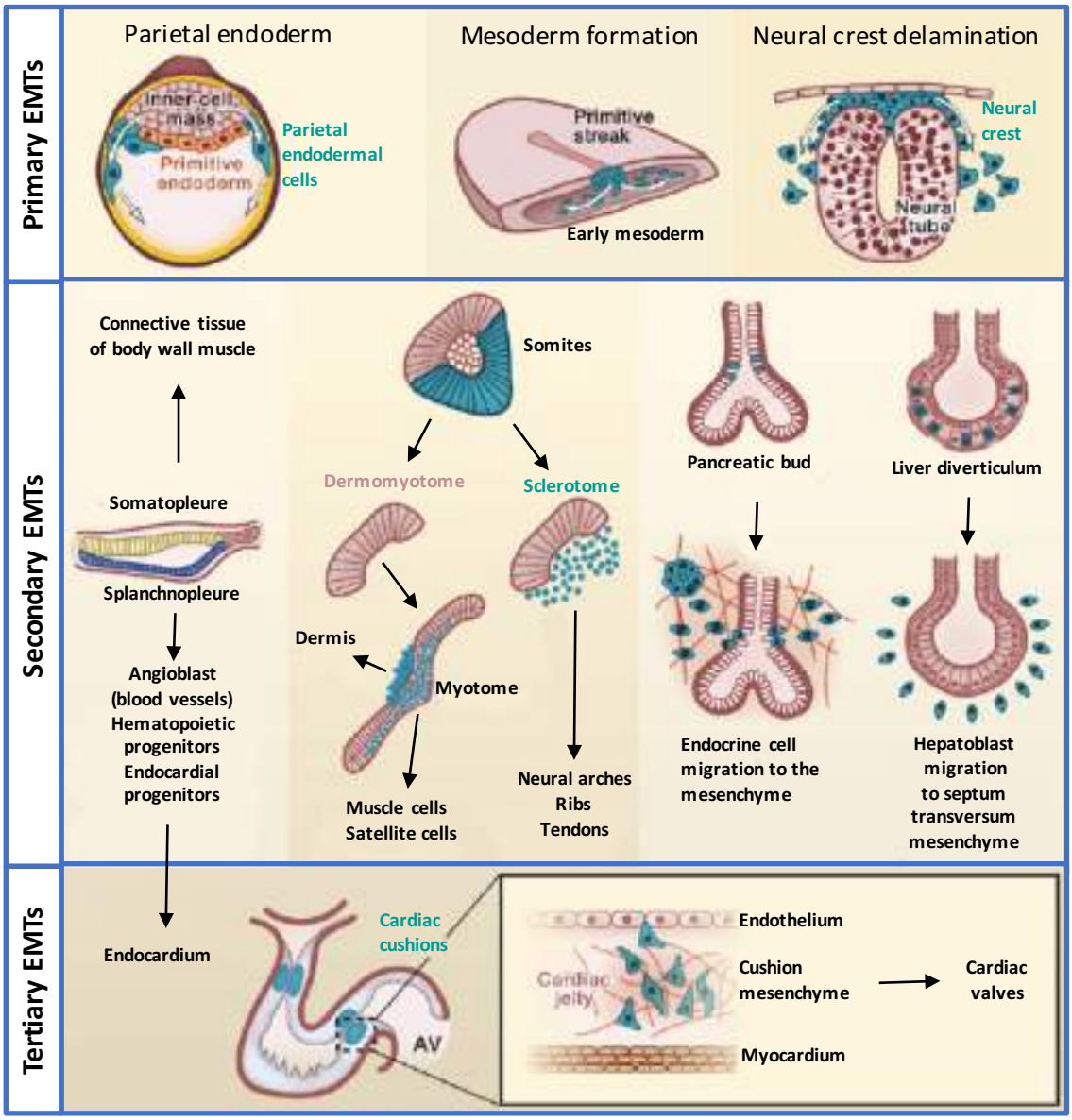

Figure 10. EMT process during embryonic development. Primary EMTs occur during early embryonic development, even before implantation. The first EMT undergone by the embryo proper occurs during gastrulation, the delamination of mesendodermal progenitors. Then, the neural crest cells delaminate from the dorsal neural tube. Thereafter, the mesodermal precursors migrate to occupy different positions along the mediolateral axis of the embryo and upon undergoing MET generate the notochord, the somites and the somatopleure and splenchnopleure. The majority of these epithelial derivatives undergo a second round of EMT as it occurs in the pancreas and the liver to induce the dissociation of endocrine cells and hepatoblasts from their respective epithelial primordia. A tertiary EMT arises during the formation of the cushion mesenchyme, which is the precursor of the cardiac valves (Adapted from Acloque et. al., 2009).

I.3.2 Epithelial-Mesenchymal Transition Inducers

I.3.2.1 Snail1

The Snail superfamily consists of two families: Snail and Scratch, with three members of the Snail superfamily described in vertebrates: Snail1, Snail2 y Snail3 (Barrallo-Gimeno and Nieto 2005). *Snail* genes encode zinc finger transcriptional repressors that are key regulators of EMT, including the transitions in both embryonic development and epithelial tumours (Barrallo-Gimeno and Nieto 2005; Cano et al. 2000). Snail1 represses the transcription of epithelial markers, including that of *E-cadherin* and *claudins* genes (Kalluri and Weinberg 2009). *Snail1* knockout mice cannot survive after gastrulation stages (Carver et al. 2001), and it has also been implicated in left–right asymmetry. As such, Snail1 downregulation shows heart *situs* defects in chicken and mice (Isaac et al. 1997; Murray and Gridley 2006), but the mechanism behind that was not known. Snail1 also controls the asymmetric development of the proepicardium on the right-side of the chick embryo (Schlueter and Brand 2009). The expression of Snail1 in breast carcinomas is associated with invasion, tumour recurrence and poor prognosis (Blanco et al. 2002; Come et al. 2006) and Snail1 drives renal fibrosis by inducing a partial EMT in mice (Grande et al. 2015).

I.3.2.2 Paired related homeobox 1: Prrx1

Prrx genes, like *Pitx* genes, belong to the paired-like homeobox transcription factors (Ploski et al. 2004). In tetrapods, the *Prrx* family includes *Prrx1* and *Prrx2* (Galliot et al. 1999). *Prrx1* displays alternative splicing to give rise to two isoforms, long and short. The long isoform of *Prrx1* contains the paired-like, the OAR and the DNA-binding domains whereas the short lacks the OAR domain. The structure of *Prrx2* is similar to *Prrx1* long (Norris and Kern 2001). However, the genome of zebrafish contains two *prrx1* genes called *prrx1a* and *prrx1b*, result of the extra whole genome duplication in teleosts (Hernandez-Vega and Minguillon 2011). *prrx1b* is closer to tetrapod *Prrx1* both in synteny and splisoforms, while *prrx1a* only presents the long isoform (Braasch et al. 2014).

Prrx1 expression is restricted to the mesoderm during embryogenesis, particularly in craniofacial regions and branchial arches, as well as in mesenchymal cells of the developing limbs (Cserjesi et al. 1992; Norris and Kern 2001). Prrx1 is also important in the differentiation of bone, muscle, and other tissues of mesodermal origin (Nohno et al. 1993). In addition, Prrx1 has also been involved in pancreatic development and regeneration in the mouse (Reichert et al. 2013), and in the maintenance of adult neurogenesis in mammals (Shimozaki et al. 2013). In the lab, we have found that Prrx1 behaves as a novel EMT inducer both in embryos and in cancer cells (Ocaña et al. 2012), where it behaves as an inducer of the mesenchymal phenotype. Importantly, Prrx1 needs to be downregulated for metastasis to form, reinforcing the idea that non-plastic mesenchymal cells cannot form metastatic outgrowths (Nieto et al. 2016).

I.4 The Role of Prrx1 in Heart Positioning in the Zebrafish

In the lab, we have recently found that a signalling pathway more prominent on the right drives heart looping in zebrafish. This novel pathway is controlled by a BMP-mediated L/R asymmetric activation of *Prrx1* in the LPM. Indeed, *prrx1a* is transiently expressed in the LPM with higher levels on the right, including the cardiogenic precursors of the second heart field that migrate toward the posterior pole of the primary heart tube located in the midline (Figure 11A). Interestingly, *prrx1a* downregulation impairs cells migration and leads to mesocardia (Figure 11B). In wild type embryos, *prrx1a* asymmetric expression activates a L/R asymmetric EMT and cell migration that generates asymmetric forces, leading to a leftward displacement of the cardiac posterior pole (Figure 12C). At the cellular level this implies the formation of an actomyosin cable, which is fundamental to exert the necessary force for the displacement (Ocaña et al. 2017).

In summary, while a left-handed Nodal-Pitx2 axis promotes and stabilizes left identify (Raya and Izpisua Belmonte 2006), a prominent right-handed BMP-mediated pathway provides instructive information that drives heart looping (Ocana et al. 2017). Thus, two parallel pathways driven by two TGF-β superfamily members (Nodal and BMP) converge in the activation of two OAR-containing transcription factors, Pitx2 and Prrx1, that integrate left-right information (Figure 11D).

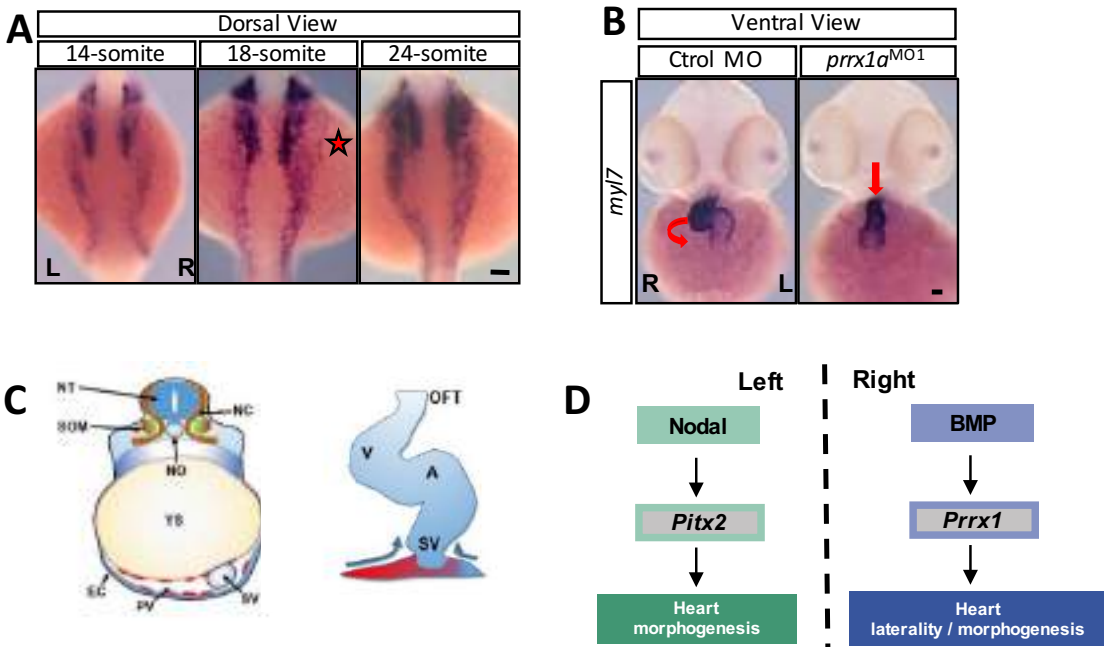

Figure 11. The asymmetric expression of *prrx1a* is essential for heart looping. (A) Transient asymmetric expression of *prrx1a* in the LPM. (**B**) Heart *situs* in control (Ctrol MO) and *prrx1a* morphant (*prrx1a*^{MO1}) embryos analyzed 50 hpf by *in situ* hybridization with a myosin light-chain 7 (*myl7*) probe. Observe the mesocardia induced after *prrx1* downregulation. **(C)** Cartoon depicting the expression of Prrx1 (red). In addition to the L/R asymmetric expression in the LPM and heart precursors, *prrx1* is symmetrically expressed in somites (SOM) and neural crest cells (NC). Proposed model for heart looping in the zebrafish. The L/R asymmetric movement of Prrx1a positive cells promote a leftward displacement of the cardiac venous pole and the asymmetric involution (blue arrows) of the pericardium. **(D)** Two parallel Nodal and BMP pathways during heart looping in zebrafish. EC, ectoderm; NO, notochord; NT, neural tube; PV, pericardial vesicle; YS, yolk sac; SV, *sinus venosus*; OFT, outflow tract; A, atrium; V, ventricule. Red star, area of asymmetry. Scale bars, 50 µm.

II. OBJECTIVES

The establishment of L/R asymmetry is fundamental for embryonic patterning and at the time of organogenesis, it plays a fundamental role in their morphogenesis and position. The first L/R symmetry breaking is highlighted by a leftward Nodal flow during gastrulation (Okada et al. 2005). Asymmetric Nodal expression induces Pitx2 on left LMP that subsequently instructs left-specific information and controls asymmetric organisation of internal organs (Raya and Izpisua Belmonte 2006). This pathway is repressed on the right-hand side by the EMT inducer Snail1. Thus, it seemed that conferring or repressing left-handed information is key in L/R determination. However, in the lab, we have recently observed that an equivalent instructive pathway more prominent from the right drives heart looping in zebrafish (Ocana et al. 2017). As such, BMP-mediated differential activation of another transcription factor, *prrx1a,* displaces the primary heart tube from the midline and induces looping.

In this context, the aim of this thesis project is to

1. Analyse whether this BMP-mediated cascade is also involved in heart looping in other vertebrates. In other words, whether the mechanism that we have observed is conserved during evolution.

2. Examine whether this pathway is also involved in the asymmetric positioning of other internal organs.

III. MATERIALS AND METHODS

III.1 Embryos

Zebrafish strains AB wild-type, Tg(*XlEef1a1:gut GFP*)^{s854} to visualize the gut, liver and pancreas *in vivo* (Field et al. 2003) and Tg*(hand2:eGFP)* to visualize Hand2^{+} cells (Yin et al. 2010) were maintained at 28 °C under standard conditions, and the embryos were staged as described previously (Kimmel et al. 1995). Fertilized hen eggs were purchased from Granja Gilbert (Tarragona, Spain) and incubated in a humidified incubator at 37.5 ºC. Chick embryos were staged according to Hamburger and Hamilton (HH) (Hamburger and Hamilton 1992) or somite number. Normal mouse embryos were obtained from natural matings of C57BL/6J mice. The age of mouse embryos was determined as days postcoitum (dpc) and by somite number. *Snai1*$^{tm1.1Stjw}$*;Tg(UBC-cre/ERT2)*^{1Ejb}*;Gt(ROSA)26Sor*$^{tm14(CAG-tdTomato)Hze}$ (*Snail1*$^{fl/fl}$; Rowe et al. 2009); ubiquitin-driven Cre/ERT2 (Ruzankina et al. 2007); tdTomato-Cre reporter (Madisen et al. 2010) embryos were obtained from pregnant females that were gavage-fed 250 µl of 30 mg ml^{-1} tamoxifen dissolved in 5% ethanol in corn oil (Sigma-Aldrich) at 6.5 dpc. Embryos were obtained at 8.5 dpc. This combined genotype circumvents the early lethality caused by the loss of function of Snail1 before gastrulation (Carver et al. 2001). *UBC-cre/ERT2* provides a temporal control of Cre activity, the presence of tamoxifen at 6.5 dpc allows Cre activity after gastrulation in all the cells of the embryo. Tamoxifen-induced Cre activity was monitored by the presence of tdTomato fluorescence. An additional *Snail1*-conditional mutant model in which deletion was driven by the Meox-Cre line (*Snail1* deleted in embryonic tissues from around 8 dpc) has been used previously (Murray and Gridley 2006). In both conditional models, SNAIL1 is deleted after early gastrulation and early L/R determination, and coinciding with the time when Snail1 is transiently expressed in a L/R asymmetric manner in the LPM (Sefton et al. 1998). Both models show heart laterality defects and our data provide the cellular and molecular mechanism that explains this phenotype.

All animal studies were performed without randomization to form the experimental groups. Sample size was not predefined for experiments involving embryos. No blinding was used in the experimental design; however, results were independently scored by two people. No selection of sex of the animals was performed,

because in all cases the embryos were younger than the sex-determination stage. All the experimental animals used here were at embryonic stages.

All animal procedures were conducted in strict compliance with the European Community Council Directive (2010/63/EU) and Spanish legislation. The protocols were approved by the CSIC Ethical Committee and the Animal Welfare Committee at the Institute of Neurosciences.

III.2 Morpholinos and mRNA Injections

All antisense morpholino oligonucleotides were obtained from Gene Tools LLC and used as described elsewhere (Nasevicius and Ekker 2001). To interfere with endogenous expression, one-cell zebrafish embryos were injected with 4 ng of a *prrx1a*^{MO} splice site blocking morpholino. The standard control morpholino from Gene Tools was used in control injections. Sequences can be found in Supplementary Table 2.

III.3 Electroporation of siRNAs, Morpholinos and Vectors

Chick embryo explants (stage HH3-4) were placed ventral side up on filter paper rings. A solution containing expression plasmids (2 mg/ml in PBS with 0.1% Fast Green and 6% sucrose), siRNAs or morpholinos (MOs at 1 μM in PBS together with 1 μg/μl pCX plasmid, 0.1% Fast Green and 6% sucrose) was injected between the vitelline membrane and the epiblast. An anodal electrode was placed over the ventral side of the embryo to cover the injected area. A train of electric pulses (5 pulses, 4 V, 50 ms, 0.5 Hz) was applied using an Intracept TSS10 pulse stimulator (Intracel). Unilateral and bilateral electroporations were performed as indicated in figure legends. For unilateral electroporation, embryos were injected with plasmid and/or siRNA into the left or right half sides and the positive platinum electrode was placed parallel to the primitive streak onto the samples. To electroporate the whole population of cardiomyocyte precursors, the positive platinum electrode was placed transverse to the primitive streak after sample injection. For gain of function experiments, pMT-cNodal (4 μg/μl; a generous gift from Dr Claudio Stern or the previously described pCX-*Prrx1* vector (1μg/μl) plus pCX-eGFP plasmid (0.5 μg/μl) were unilaterally electroporated. Control embryos were

electroporated with the pMT or pCX empty vectors plus pCX-eGFP. For loss of function experiments two siRNA for Prrx1 were designed (See table 2 for sequences). A mix of these siRNAs (2μM each), plus the pCX-eGFP plasmid (0.5 μg/μl) and 6% sucrose was injected and electroporated unilateral o bilaterally as indicated in the figure legends. Control embryos were electroporated with a scrambled siRNA. To interfere with *Snail1* expression two splice site-blocking fluorescein-labelled morpholinos were designed ($gSn1^{MO1}$ and $gSn1^{MO2}$ Sequences in table X) and a mix of them (1mM each) was electroporated alone or in combination with the two siRNA for Prrx1 and pCX-RFP as a control for electroporation. The standard fluorescein-labelled control morpholino from Gene Tools was used as a control. The efficiency of *Snail1* MOs in preventing splicing was tested by RT-PCR as described above. Oligonucleotides in exons 1 and 2 for $Snail1^{MO1}$ that yield a fragment of 255 bp, and in exon 2 and 3 for $Snail1^{MO2}$ that yield fragments 288 bp were used. The unspliced fragments are 950 and 1244, respectively.

III.4 In Situ Hybridisation

Whole-mount *in situ* hybridization was carried out as described previously (Nieto et al., 1996) omitting the proteinase K treatment. Digoxigenin-labelled probes were synthesized from full-length chicken or mouse cDNAs and subcloned into the pGEMT-easy vector (Promega) or pCDNA3 (Thermo Fisher) with the primers indicated in Table 2. Hybridized probes were detected using an alkaline phosphatase-conjugated anti-digoxigenin antibody (Roche, 1:1000) in the presence of NBT/BCIP substrates (Roche). For whole-mount fluorescent *in situ* hybridization, probes were labeled using digoxigenin- or fluorescein-coupled nucleotides (Roche, 1:1000) and were sequentially developed with POD-conjugated anti-fluorescein or anti-digoxigenin antibodies (Roche). Peroxidase activity was successively detected with the TSA-plus Cy3 and Fluorescein kits (Perkin Elmer). In some cases, the embryos were subjected to immunostaining with anti-GFP antibody (Invitrogen, 1:1000). After hybridization and/or immunohistochemistry, embryos were fixed in 4% paraformaldehyde in PBS, washed, and photographed. Some embryos were embedded in paraffin, gelatine or low melting temperature agarose and sectioned at 7, 40 or 150 μm, respectively.

III.5 Immunofluorescence Staining

Whole mount embryos were fixed with 4% PFA overnight at 4 °C. After fixation, the embryos were dehydrated and rehydrated in gradual PBT (PBS + 0.1 % Tween 20): methanol series. Antigen retrieval was performed by maintaining the embryos for 15 min at 70 ºC in 150 mM Tris-HCl buffer (pH 9) that were then permeabilised with cold acetone for 20 min at -20ºC. After washing with PBT, embryos were blocked with 10 % FBS for 3 hours at room temperature and incubated with the primary antibodies overnight at 4 °C. After washing for several hours in PBT, the embryos were incubated with the secondary antibodies overnight at 4 °C. Some embryos were embedded in gelatin or low melting temperature agarose and sectioned at 150 µm. For immunofluorescence on sections, embryos were embedded in paraffin and sectioned at 7 µm. Immunostaining was performed by standard procedures. Antigen retrieval was performed on the paraffin sections by incubation for 20 min at 100 ºC in Sodium Citrate Buffer (10 mM Sodium Citrate, 0.05% Tween 20, pH 6.0). Sections were incubated with the primary antibodies overnight at 4ºC and then incubated with the secondary antibodies for 1 hour at RT. For antibody details, see Table 1.

Detection of stress fibres and actin was performed using either TRITC- or FITC-conjugated phalloidin. Fixed embryos were treated with a 1:50 dilution of labelled Phalloidin in PBT at 4 °C overnight. After extensive washing in PBT, embryos or sections were directly analysed on the confocal microscope

III.6 RNA Extraction, cDNAs Isolation and RT-qPCR Analysis

Using the Illustra RNAspin Mini isolation kit (GE Healthcare 25-0500-70), total mRNA was extracted from pools of 10 zebrafish embryos at 48 hpf, from pools of 5 chick embryos at HH11 stage or from mouse embryos at 8.5 dpc. Reverse transcription of total RNA was performed using Maxima First Strand cDNA Synthesis Kit for RT-qPCR (Thermo Scientific), according to the manufacturer's guidelines. RT-qPCRs were performed in a Step One Plus machine (Applied Biosystems) using Fast SYBR Green Mastermix (Applied Biosystems). RNA expression levels were calculated using the comparative Ct method normalized to the internal control genes indicated below. The final results were expressed as the relative RNA levels, calculated with the $2^{-(\Delta\Delta Ct)}$

method. Data are represented as the mean±s.e.m. of at least three independent experiments with each point analysed in triplicate. The primers used are listed in Table 2.

Table 1. Antibodies used in this work.

Primary Antibodies	Source	Catalog Number	Dilution
Anti-GPF-chicken	Aveslab	GFP-1020	1/500
Anti-RFP-mouse	Life technologies	MA515257	1/500
Phalloidin-TRITC	Sigma	P1951	1/50
Phalloidin-FITC	Sigma	P5282	1/50
Anti-Prrx1-rabbit	Tanaka lab	-	1/200
Anti-S46-mouse	Hybridoma bank	-	1/250
Anti-MF-20-mouse	Hybridoma bank	-	1/250
Anti-Islet1-mouse	Hybridoma bank	40.2D6	1/500
Anti-Palladin-mouse	Thermo Fisher Scientific	MA5-16141	1/50
Anti-Fluorescein-POD	Roche	11 426 320 001	1/500
Secondary Antibodies	**Source**	**Catalog Number**	**Dilution**
Alexa Fluor 488 goat anti-chicken	Life technologies	A11039	1/500
Alexa Fluor 488 goat anti-mouse	Invitrogen	A11001	1/500
Alexa Fluor 488 goat anti-rabbit	Invitrogen	A11008	1/500
Alexa Fluor 568 goat anti-mouse	Invitrogen	A11004	1/500
Alexa Fluor 568 goat anti-rabbit	Invitrogen	A11011	1/500
Alexa Fluor 647 goat anti-rabbit	Life technologies	A27040	1/500
Alexa Fluor 647 goat anti-mouse	Life technologies	A31571	1/500

III.7 Microscopy and Image Analysis

Whole-mount *in situ* images were taken using a Leica M125 dissecting scope and sections photographed using a Leica DMR microscope under Nomarski optics and equipped with a Leica DFC 7000T digital camera. *In situ* and immunofluorescence

images were collected on an Olympus FV1200 microscope with a 20x objective (UPLSAPO 0.75NA dry) a 40x objective (UPLFLN 1.30 oil) and a 60x objective

(PLANAPO 1.40 oil). Different fluorophores were excited with the indicated laser lines as follows: DAPI at 405 nm, GFP, FITC and Alexa Fluor 488 at 488 nm, Cy3, RFP and Alexa Fluor 568 at 559 nm and Alexa Fluor 647 at 635 nm. DAPI was collected at 440-470 nm, GFP, FITC and Alexa Fluor 488 at 500-550 nm, Cy3, RFP and Alexa Fluor 568 at 570-620 nm and Alexa Fluor 647 at 650-700 nm. Raw data were analyzed using Imaris software (Bitplane AG), to create 3D and 4D reconstructions of different views and for surface rendering.

III.8 Statistical Analysis

Statistical analysis was performed using the GraphPad Prism software package. Results were expressed as mean s.e.m. (standard error of mean). Differences among groups were tested by using two-tailed pair or unpaired Student's t-test or one-way ANOVA test, as indicated in figure legends. Differences were considered statistically significant when $*p < 0.05$, $**p < 0.01$, $***p < 0.001$.

Table 2. Oligos used in this work.

Name	Sequence 5´-3´	Type
***prrx1a*^{MO1}**	TTTTGTTCTCCAGCACTTACTCTCC	Morpholino
***Snail1*^{MO1}**	CCAGCACTGTAGGCAACAGGCAGCA	Morpholino
***Snail1*^{MO2}**	GCCAAGTAGCGTCATTACCAGTGTG	Morpholino
gSnai1PF1	GCAAGAAGCCCAACTACAGC	RT-PCR
gSnail1PR1	TGCCCTCATCCTCCTCACTA	RT-PCR
gSnail1PF2	CCCTGTGTCTGCAAGATGTG	RT-PCR
gSnail1PR2	ATGTATCTGCACGGGAAAGG	RT-PCR
zfgapdh-F	GTACGACTCCACCCATGGAA	RT-PCR
zfgapdh-R	CCTGCATCACCCCACTTAAT	RT-PCR
siRNA1-Prrx1	UUGGCUUGUAAAUUGUCCAGGCCGG	siRNA
siRNA2-Prrx1	GGACAAUGAUCAGCUGAAUUCAGAA	siRNA
cAmhc F	ACTGGATGCTGAGACACGAA	Probe cloning
cAmhc R	TCAGAGATTGGGGCTGGAAG	Probe cloning
cVmhc F	TGCAGTCCACCCTTGATTCT	Probe cloning
cVmhc R	TCCCTTGACTTGCTCCTCAG	Probe cloning
cPalld F	TGATGGAACTTGCTCACTGC	Probe cloning
cPalld R	GCTTGGTTGTTTGAGGTGGT	Probe cloning
cTbx18 F	AGGGGATGAGTGTAGGGTCT	Probe cloning
cTbx18 R	CTTCTTGGAGCGTTCGGATG	Probe cloning
cAmhc F	ACTGGATGCTGAGACACGAA	Probe cloning
cAmhc R	TCAGAGATTGGGGCTGGAAG	Probe cloning
cVmhc F	TGCAGTCCACCCTTGATTCT	Probe cloning
cVmhc R	TCCCTTGACTTGCTCCTCAG	Probe cloning
cTbx5 F	GTGGGGACGGAGATGATCAT	Probe cloning
cTbx5 R	GAGCTGGCGTACATACATGC	Probe cloning
cNkx2.5 F	CATGTTGGCCACCTTCAAGC	Probe cloning
cNkx2.5 R	ATGAGTTGTAGGGCTTGGCT	Probe cloning
MmPrrx1 F	GACCATGACCTCCAGCTACGG	Probe cloning
MmPrrx1 R	TCAGTTGACTGTTGGCACCT	Probe cloning
MmPrrx2 F	GCAAGAACTTCTCGGTGAGC	Probe cloning
MmPrrx2 R	GCCTTAGGCACAATCTCAGC	Probe cloning
***GgRS*17F**	ACACCCGTCTGGGCAACGACT	qRT-PCR
***GgRS*17R**	CCCGCTGGATGCGCTTCATCA	qRT-PCR
GgPrrx1F	CACTACCCCGATGCCTTTGTA	qRT-PCR
***GgPrrx1* R**	GAAACTTGGCTCTCCGGTTCT	qRT-PCR
GgPalladin F	GCAGCGCACAACTAACTGTC	qRT-PCR
GgPalladin R	TGGGAAATGGTGGAAATCAT	qRT-PCR
MmEef2 F	AGCGAGGACAAAGACAAGGA	qRT-PCR
MmEef2 R	TACTTCTGTGCAGTGACGGG	qRT-PCR
MmSnail1 F	CAGCTGCTTCGAGCCATAGA	qRT-PCR
MmSnail1 R	TAGGGGAGGTAGGGAAGTGG	qRT-PCR
MmPalladin F	GTCGCGTCAGTTGTACAGGA	qRT-PCR
MmPalladin R	CACTGTCCCGTGATCGAGAG	qRT-PCR
***DrEF1α* F**	GTCAAGGACATCCGTCGTG	qRT-PCR
***DrEF1α* R**	ACCAGGGTGGTTCAGGATG	qRT-PCR
***Drprrx1a* F**	AGTCTCCGGGACTCACCAG	qRT-PCR
***Drprrx1*a R**	TCTCCTCTGCGTTGAGCTG	qRT-PCR

IV. RESULTS

IV.1 Heart Positioning in the Chick Embryo

IV.1.1 Expression Pattern of Prrx1 in the Chick

In the zebrafish embryo *prrx1a* is expressed in the LPM in a L/R asymmetric manner with higher levels on the right, which is essential for heart looping (Ocaña et al. 2017). Thus, we wonder whether *Prrx1* was also asymmetrically expressed in the chick embryo at similar stages. We performed whole-mount *in situ* hybridization using specific probes for *Prrx1* at different stages and we also observed higher levels on the right LPM. This asymmetric expression occurs in a narrow temporal window corresponding to stages from 6 to 11 somites (Figure 12A).

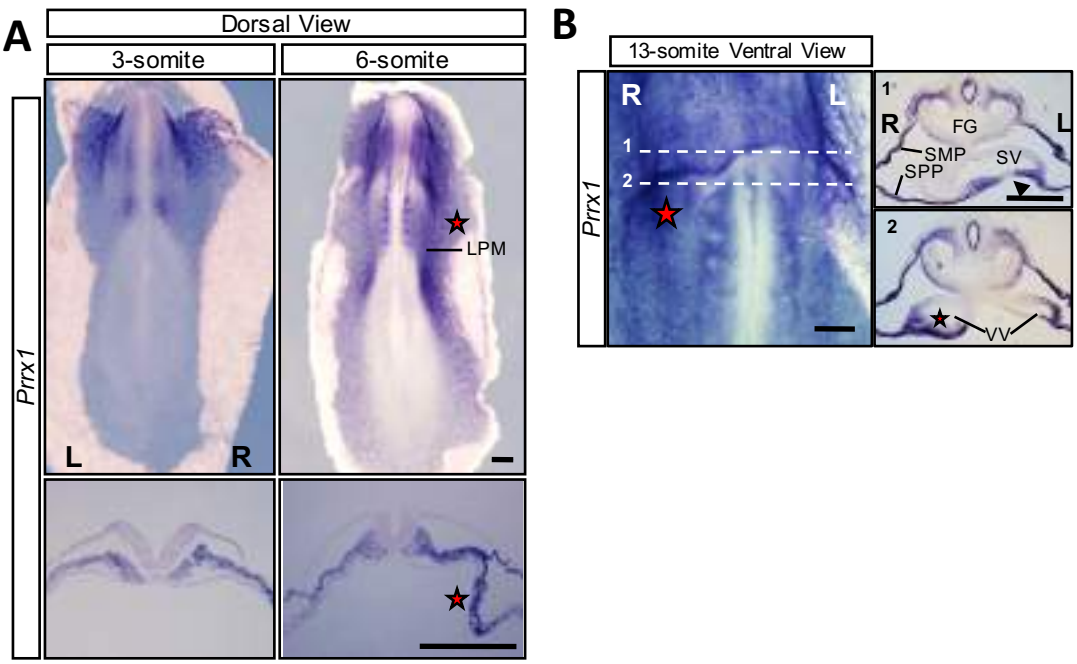

Figure 12. The asymmetric expression of *Prrx1* in chicken. (**A**) *Prrx1* is asymmetrically expressed in the chick embryo LPM, as seen in whole embryos and transverse sections. The red stars highlight areas of asymmetry. (**B**) Ventral view of a 13 somite-stage whole mount chicken embryo and transverse sections showing the asymmetric *Prrx1* expression in the *sinus venosus* (SV) and the vitelline veins (VV). The arrowhead shows the center of the venous pole displaced to the left. Scale bars, 250 μm.

We next examined *Prrx1* expression in the developing heart and found that *Prrx1* is also asymmetrically expressed in the *sinus venosus* and vitelline veins at 13-somite stage (HH 11; Figure 12B). Then, to better assess *Prrx1* expression in different cardiac cell populations, we compared the expression of *Prrx1* with those of *Nkx2.5* and *Tbx5* at 5-somite and 13-somite stages by double fluorescent *in situ* hybridisation. Nkx2.5 is a homeodomain-containing transcriptional activator expressed in the primary heart tube, and its expression is essential for the development of atrium and ventricle, and for the formation of the atrioventricular (AV) valve (Akazawa and Komuro 2003). Tbx5 is a T-box transcription factor with a conserved role in vertebrate heart development, and it is expressed in the atrium and ventricle and in the cells that contribute to the posterior/venous pole (Xie et al. 2012). We observed that *Prrx1* is not expressed in the primary heart tube PHT, which is *Nkx2.5* positive, but that it is expressed by a population of *Tbx5*+ cells lateral and posterior to the cardiac venous pole (Figure 13).

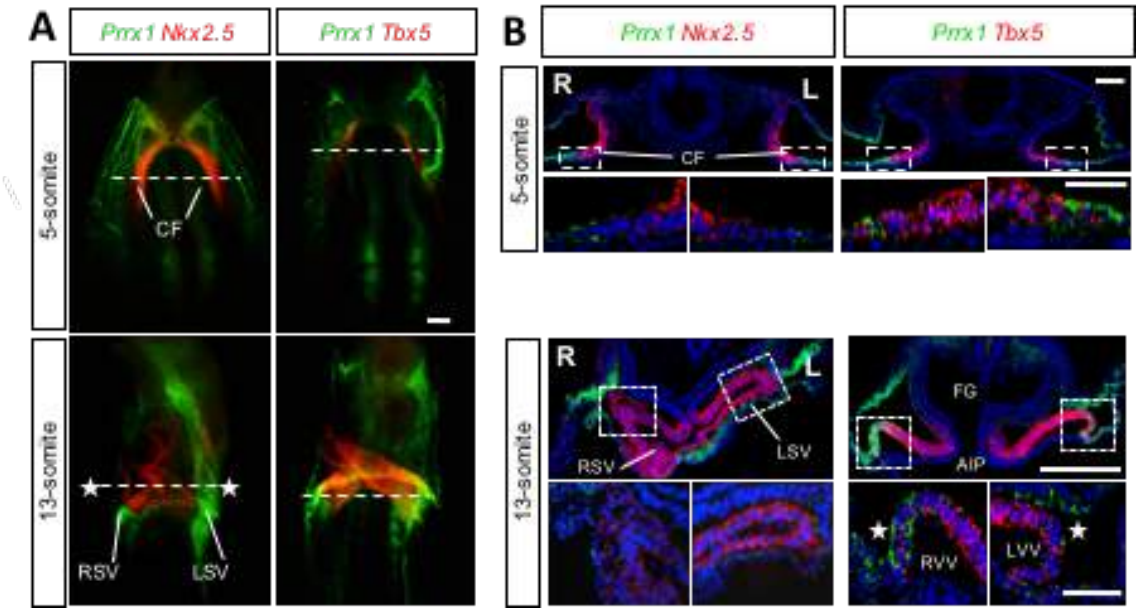

Figure 13. *Prrx1* is expressed by the cells lateral and posterior to the cardiac venous pole in the PHF in chicken. (**A**) Ventral view of whole chick embryos to show the expression of *Prrx1* (green) and *Nkx2.5* (red) or *Tbx5* (red). The yellow stars indicate the areas of Tbx5/Prrx1 double-positive cells. The dotted lines indicate the levels of the transverse sections shown in b (5 somite-stage) and in Fig. 4c (13-somite stage). (**B**) Transverse sections showing *Prrx1* (green) and *Nkx2.5* (red) or *Tbx5* (red) expression. At this stage Prrx1 has a mutually exclusive distribution with both *Nkx2.5* and *Tbx5*. AIP, Anterior intestinal portal; CF, cardiac fields; FG, Foregut; LRH, left

sinus venous horn; RSH, right sinus venous horn; RVV, right vitelline vein; LVV, left vitelline vein. Scale bars, 100 µm.

We performed double fluorescent *in situ* hybridisation using specific probes for the atrial (aMHC) or ventricular (vMHC) myosin to check whether *Prrx1* was expressed by cardiomyocytes, and we did not observe any *Prrx1* expression in the myocardium (Figure 14).

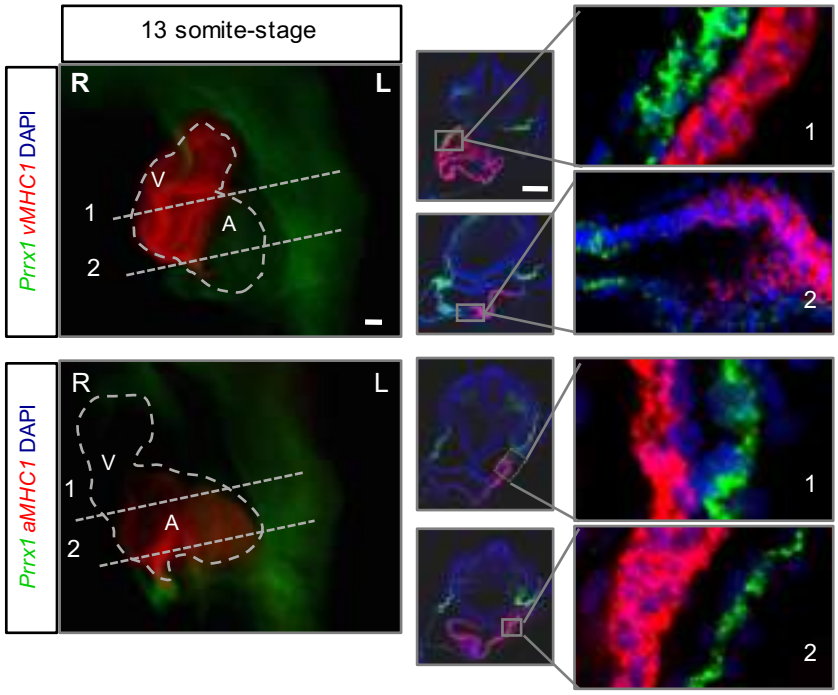

Figure 14. *Prrx1* is not expressed in the myocardium. Ventral views of whole 13 somite-stage chick embryos subjected to dual fluorescent *in situ* hybridization to assess the expression of *Prrx1* with respect to the atrial (aMHC) or ventricular (vMHC) myosins that reveal the myocardium. Note the absence of myocardial *Prrx1* expression in the transverse gelatine sections. A, atrium; V, Ventricle. Scale bars, 100 µm.

Collectively, our data show that in the chicken embryo *Prrx1* is asymmetrically expressed, with higher levels in the right LPM in a narrow temporal window. In addition, *Prrx1* is also expressed in cells adjacent to the posterior pole, but not in the heart tube. Therefore, we wanted to analyse whether this asymmetric expression of Prrx1 played any role heart positioning in chick.

IV.1.2 Prrx1 Regulates Heart Looping in Chick

Once we analysed the asymmetric expression of *Prrx1* in the progenitors of the cardiac venous pole, we decided to examine whether the transient higher expression of Prrx1 could have any effect on heart looping in the chick. We performed *Prrx1* loss and gain of function experiments by electroporating different constructs. The region where cardiomyocyte precursors lie in HH3 chick embryos was bilaterally co-electroporated with an eGFP reporter construct plus either a mix of two RNAi against *Prrx1* or a control RNAi (see Methods). RNAi electroporation reduced *Prrx1* transcripts to around 40% (Figure 15A). The embryos were examined at HH12 by dual immunofluorescence for EGFP and the cardiomyocyte marker MF20 (Figure 15B). We found that the majority of embryos where Prrx1 was downregulated displayed mesocardia (No-loop 56,5 %, 56 of 99) (Figure 15C).

We further tested our hypothesis that transient higher expression of *Prrx1* in the right LPM could be responsible for heart looping. We took advantage of the electroporation technique that allows unilateral manipulation of gene expression in chick. Thus, we performed loss and gain of *Prrx1* function in the left LPM and analysed the heart *situs* in control and *Prrx1* knocked-down embryos by dual immunofluorescence for EGFP and expression of MF20. We observed that downregulation of *Prrx1* by RNAi in the left half of the embryo did not affect heart looping as 94% of the *Prrx1* RNAi electroporated embryos showed normal *situs* (15/16; Figure 15D, E). However, *Prrx1* overexpression on the left side affected heart *situs* with 36% of the embryos displaying reverse looping (Figure 15F, G).

These data indicate that transient higher expression of *Prrx1* in the right LPM is sufficient to drive heart looping. Then, we wondered whether Prrx1 had a role on heart morphogenesis.

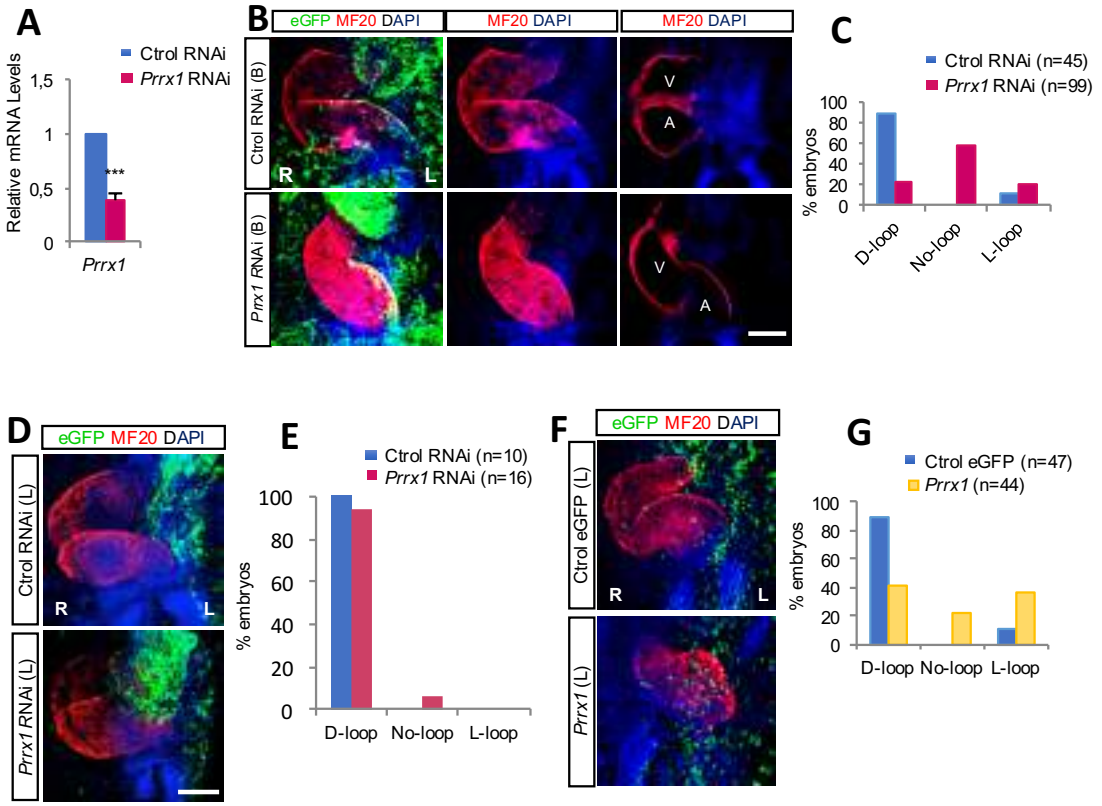

Figure 15. The asymmetric expression of *Prrx1* is essential for heart looping in chicken. (**A**) Downregulation of *Prrx1* transcription upon RNAi electroporation. Data represent mean ± s.e.m. *** p<0.001 by Student´s t-test. (**B**) The region of cardiomyocyte precursors in HH3 chick embryos was bilaterally co-electroporated with an eGFP reporter construct plus either a mix of two RNAi against Prrx1 or a control RNAi. Embryos were examined at HH12 by dual immunofluorescence for EGFP (green) and the cardiomyocyte marker MF20 (red), and they were counterstained with DAPI (blue). Left and middle panels correspond to the maximum intensity projection of confocal images. The right panel shows z-plane sections. (**C**) Quantitative analysis of heart *situs* in control and Prrx1 knockdown embryos (HH11-12; No-Loop 56,5%, 56 of 99; D-Loop 23,2%, 23 of 99; L-Loop 20,3%, 20 of 99). (**D**) Chick embryos co-electroporated with the same vectors but only on the left-hand side (L) of the embryo. (**E**) Embryos were examined for heart *situs* at HH11-12 (10/10 Control and 15/16 electroporated with *Prrx1* RNAi showed the normal D-Loop configuration). (**F**) Chick embryos similarly electroporated exclusively on the left region of the cardiomyocyte precursors area (L) with either a control vector (pCX-eGFP) or one containing the *Prrx1*-coding sequence. (**G**) Heart *situs* in embryos with *Prrx1* overexpression at HH11-12 (D-loop 41%, 18 of 44; No-loop 23%, 10 of 44; L-loop 36%, 16 of 44). Control embryos show D-loop in 42 of 47 (89%). Scale bars, 250 µm.

IV.1.3 Deficient Prrx1 Expression Affects the Posterior Pole of Heart in Chick

Having shown that L/R asymmetric Prrx1 expression drives heart looping in the chick, we examined cardiac defects after its downregulation. First, we checked whether there was any effect on atrium and ventricle. We performed double fluorescent *in situ* hybridisation using again the specific probes for the atrial (aMHC) or ventricular (vMHC) myosins and analysed control and *Prrx1* downregulated embryos. We found that deficient *Prrx1* expression did not prevent the specification of atrial and ventricular fates (Figure 16A). We carried out a morphometric analysis in the *Prrx1* RNAi embryos and detected that the size of the atrium was reduced with respect to that in control embryos (Figure 16B).

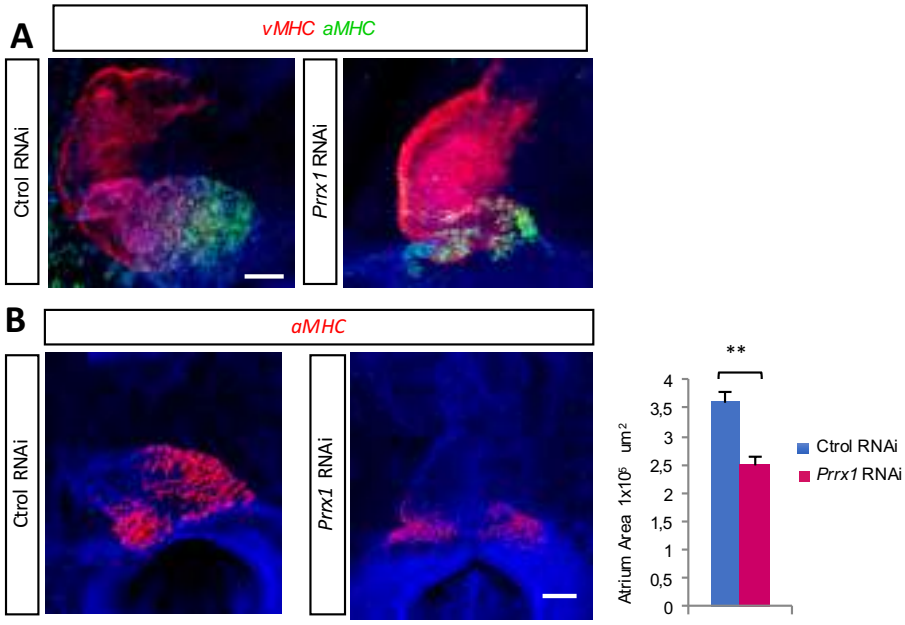

Figure 16. Downregulation Prrx1 affects cardiac phenotype in chicken. (**A**) Analysis of aMHC (green) and vMHC (red) in control embryos (Ctrol RNAi) and in those electroporated with Prrx1 RNAi. (**B**) Morphometric analysis of the atrium in chick embryos electroporated with Ctrol RNAi or *Prrx1* RNAi and analysed at stage HH11 with the atrial marker aMHC (red). Top panels show control and Prrx1 knock-down embryos hybridized with the atrial marker aMHC (red). The graph represents the area of aMHC expression (μm^2; 7 embryos per condition). Data represent mean ± s.e.m. **p < 0.01, Student t-test. Scale bars, 100 µm.

We next analyzed the defects in this structure at the molecular level, by assessing Islet1 expression, which is a marker of the posterior pole (Hami et al. 2011). Whole-mount immunofluorescence staining using Prrx1 and Islet1 antibodies indicated

that Prrx1 and Islet1 were co-expressed in the *sinus venosus* cells adjacent to the posterior pole in wt embryos (Figure 17A) and that Islet1 expression was downregulated in Prrx1 deficient embryos (Figure 17B).

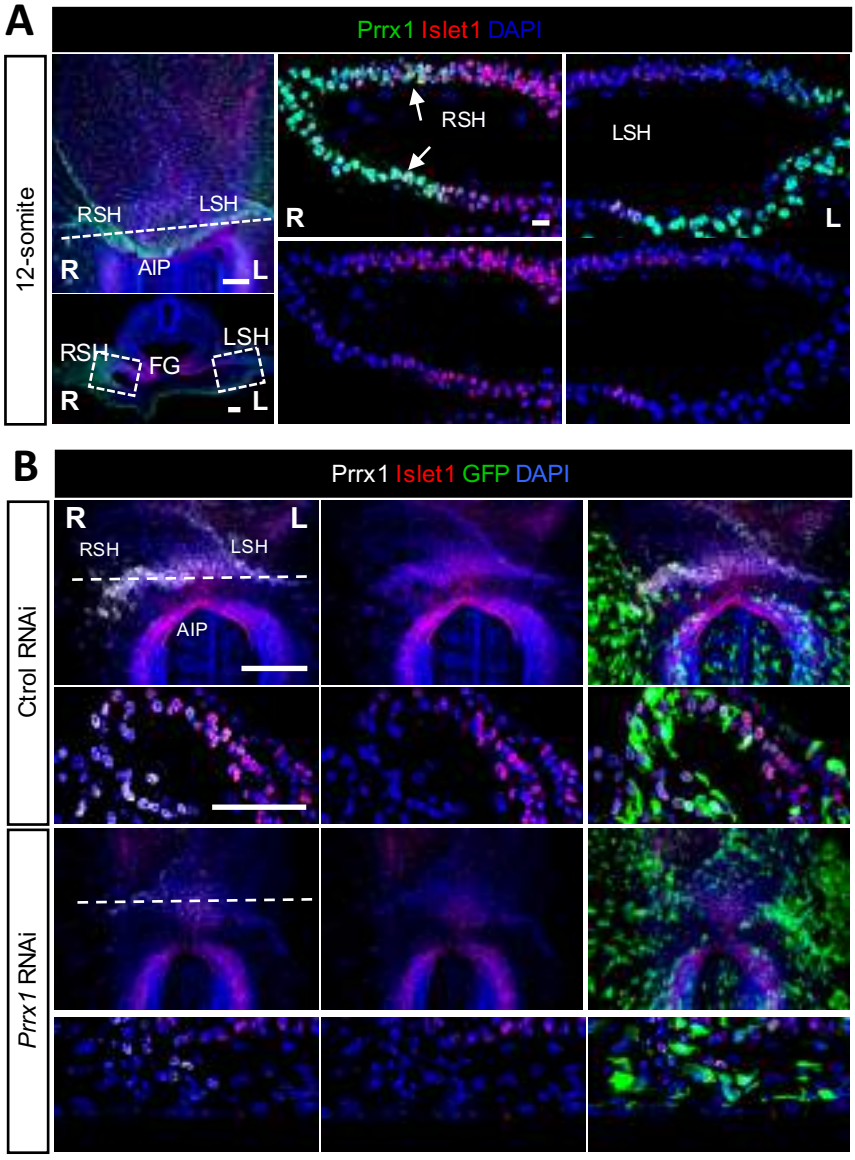

Figure 17. Prrx1 is expressed by the Islet1+ progenitors of the *sinus venosus* in chicken. (**A**) Islet1 is coexpressed with Prrx1 particularly in the right *sinus* horn (RSH) (arrows). Ventral view of a maximum intensity projection in chick embryo at 12 somite-stage. (**B**) Downregulation of *Prrx1* upon RNAi electroporation in chick embryos leads to Islet1 downregulation (71%, 5 of 7). Control RNAi does not modify Islet1 expression (n=6). Sections correspond to the right *sinus* horn at the level indicated by the dotted line. A, atrium; AIP, Anterior intestinal portal; CF, cardiac fields; FG, Foregut; LRH, left *sinus venosus* horn; OFT, Outflow tract; RSH, right *sinus venosus* horn; V, ventricle; Scale bars, 100 μm.

The posterior pole of heart includes different progenitor populations. The *sinus venosus*, one of the progenitor populations, expresses *Tbx18* and it is known to contribute to the venous pole of the heart together with the SHF, which is located more dorsomedially. This population has been referred to by different authors as posterior second heart field (Dominguez et al. 2012; Rana et al. 2014) or tertiary heart field (Bressan et al. 2013), as it is located more laterally than the classical SHF. Thus, we examined whether the domain of Prrx1 expression could include the tertiary heart field. We observed asymmetric co-expression with *Prrx1* and *Tbx18* in the *sinus venosus* horns, with higher levels on the right (Figure 18A). Interestingly, *Tbx18* expression was also diminished in *Prrx1* downregulated embryos (Figure 18B).

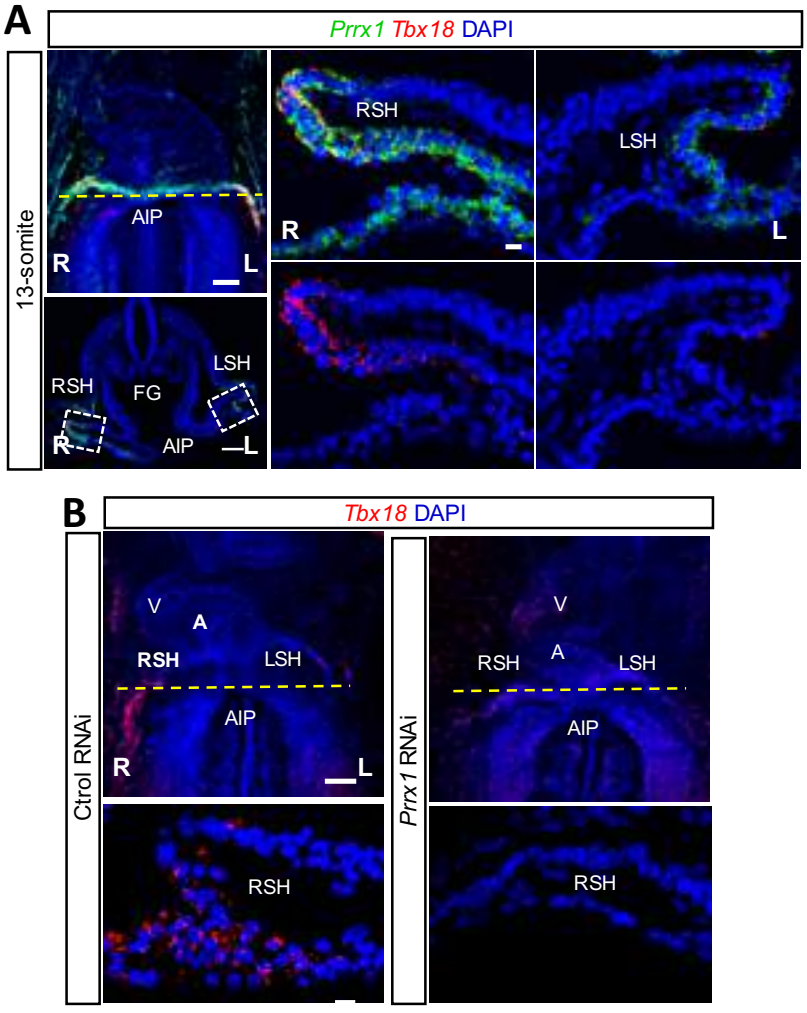

Figure 18. *Prrx1* is expressed by the Tbx18+ progenitors of the *sinus venosus* in chicken. (**A**) Ventral view of a 13-somite stage chick embryo at and transverse sections. *Tbx18* is asymmetrically expressed in the right *sinus* horn (RSH), where it is coexpressed with *Prrx1*. (**B**) *Prrx1* downregulation upon RNAi electroporation

abolishes the expression of *Tbx18* in the venous pole of the heart. A, atrium; AIP, anterior intestinal portal; FG, foregut; LRH, left *sinus* horn; OFT, Outflow tract; RSH, right *sinus* horn; V, ventricle; VV, vitelline veins Scale bars, 100 µm except for the sections shown in (A) and (B), which corresponds to 10 µm.

In conclusion, these data indicate that Prrx1 is expressed in the *sinus venosus* cells adjacent to the posterior pole, and that downregulation of Prrx1 causes defects in the posterior pole. Indeed, Prrx1 expression corresponds to tertiary heart field cells ($Tbx18^{+}$ cell population) that contributes to venous pole of the heart.

IV.1.4 Prrx1 Downregulation Disturbs the Actomyosin-Mediated Differential Forces During Heart Looping

The looping defects which we observed in chicken were compatible with previous data from the lab in zebrafish. We found that asymmetric *prrx1a* expression drives differential cell movements leading to a leftward displacement of the cardiac posterior pole. This leftward displacement promotes dextral looping through an actomyosin-dependent mechanism (Ocaña et al. 2017). Thus, we wonder whether this actomyosin-dependent leftward looping mechanism was also conserved in the chick. In this case, we performed whole mount staining for F-actin and Prrx1 in control and *Prrx1* downregulated embryos. We used phalloidin, that binds to F-actin fibers, and found that it labelled Prrx1 expressing cells at the wall of the right vitelline vein and in the ventral splanchnic lateral mesoderm (VSPLM), located at the right of the anterior intestinal portal (AIP) in control embryos (Figure 19). Significantly, Prrx1 downregulation caused a loss of F-actin and of L/R morphological asymmetry (Figure 19), compatible with the mesocardia observed.

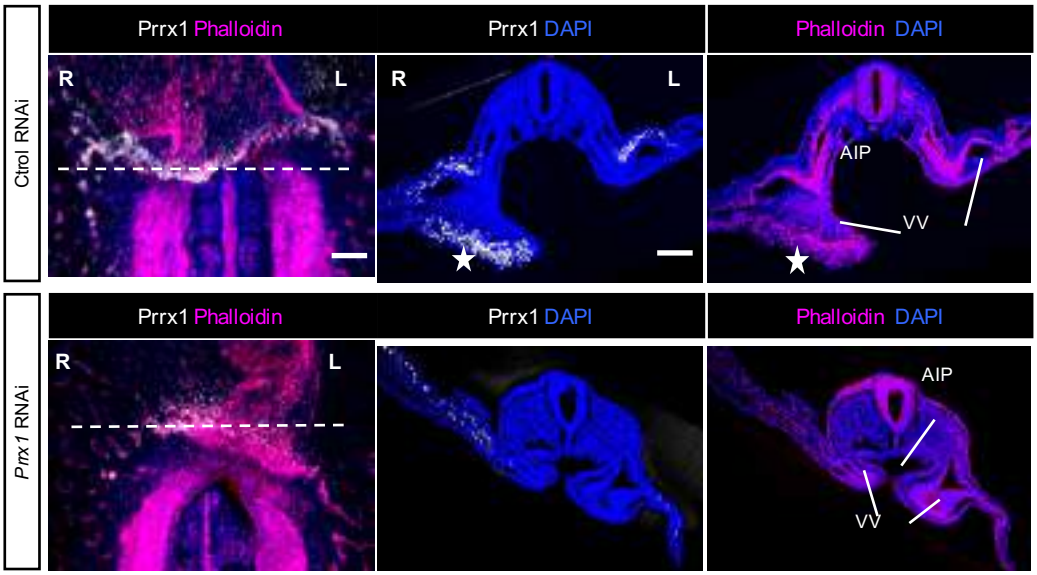

Figure 19. The asymmetric L/R Prrx1 expression is required for the formation of an actomyosin cable in chicken embryos. Prrx1 immunostaining (white) and phalloidin staining (magenta) in 13 somite-stage chick embryos electroporated with control or *Prrx1* RNAi. White stars show the region of colocalization in the right vitelline vein. Panels are maximum intensity projection of confocal images. AIP, Anterior intestinal portal; VV, vitelline veins. Scale bars, 100 µm.

Next, we wanted to get further insight into the mechanisms that link this transcription factor with the reorganization of the cytoskeleton. We found that, as in the fish (Ocaña et al. 2017), Palladin, an actin-binding protein that promotes and maintains actin bundling in migratory and invasive cells (Gurung et al. 2016; Najm and El-Sibai 2014) was co-expressed with *Prrx1* in a number of cells, and that *Palladin* expression was asymmetric and higher in the chicken right *sinus venosus* horn (Figure 20A). Then, we analysed *Palladin* expression in control and *Prrx1* downregulated embryos and found that *Prrx1* downregulation decreased the asymmetric expression of *Palladin* (Figure 20B).

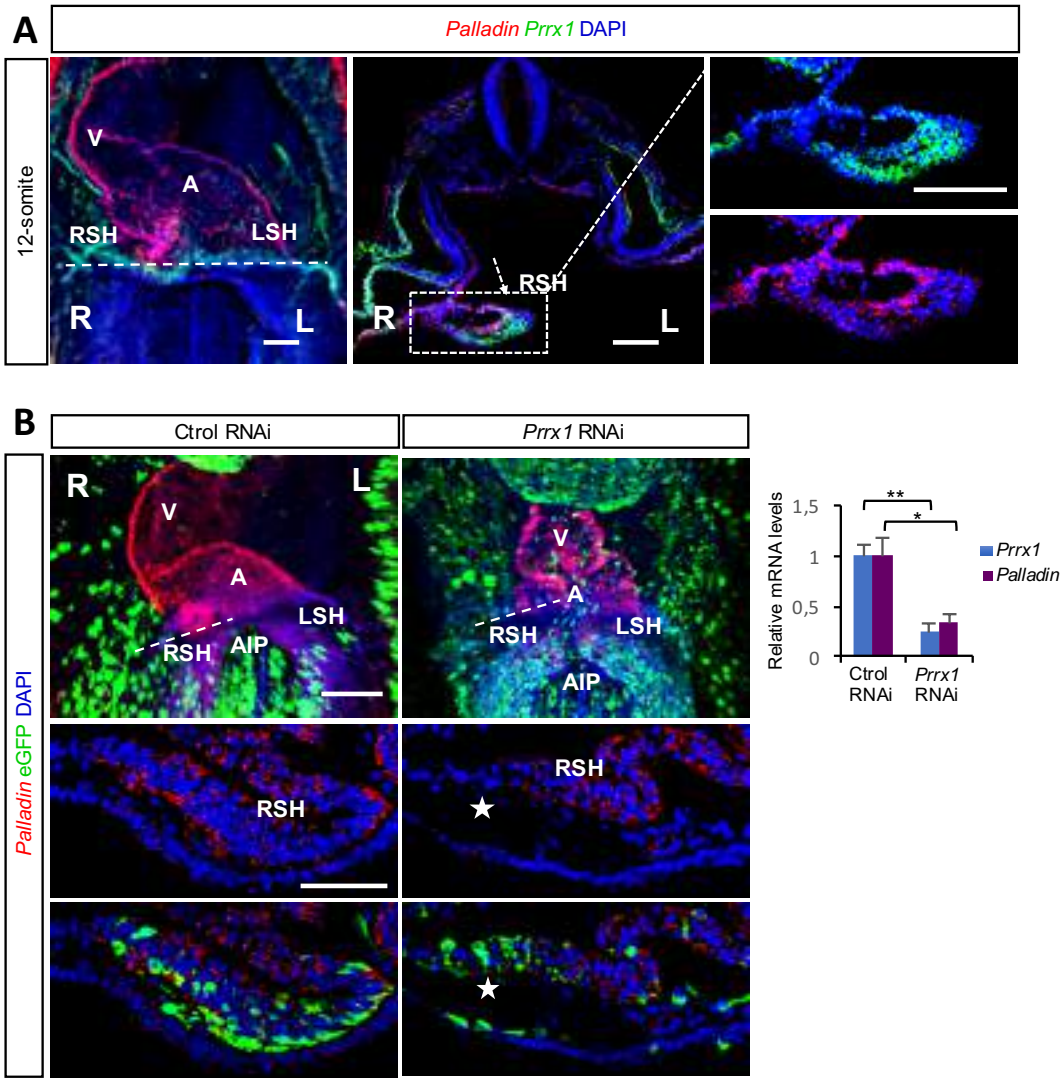

Figure 20. The asymmetric L/R Prrx1 expression regulates *Palladin* expression in chicken. (**A**) *Palladin* expression is L/R asymmetric, higher in right *sinus venosus* horn, where it is coexpressed with *Prrx1* in a number of cells (arrow). (**B**) *Palladin* expression decreases when *Prrx1* is downregulated upon RNAi electroporation (75%, 6 out of 8) but not in control RNAi (n=6). The graph shows *Prrx1* and *Palladin* expression in chick embryos electroporated bilaterally with control or *Prrx1* RNAi in the cardiac precursors at stage HH3 and analysed at HH11. Data represent mean ± s.e.m. of 4 pools (5 embryos each) of control and Prrx1 knockdown embryos. * $p<0.05$, ** $p<0.01$ by Student t-test. Dotted lines show the level of the sections. A, atrium; AIP, anterior intestinal portal; LRH, left *sinus* horn; RSH, right *sinus* horn; V, ventricle. Scale bars, 100 µm.

In conclusion, these data indicate that the asymmetric L/R Prrx1 expression in the chick is also compatible with the formation of an actomyosin cable. Thus, as in the

fish, leftward displacement and posterior looping also involves an actomyosin-dependent mechanism.

IV.1.5 Differential Contribution of Prrx1 and Snail1 Drive Heart Positioning in the Chick Embryo

Snail1 has also been implicated in the signalling cascade that confers L/R identity in the chick, with a main role in repressing *Pitx2* expression on the right (Morales et al. 2007; Patel et al. 1999; Raya and Izpisua Belmonte 2006). Interestingly, downregulation of Snail1 causes defects in heart *situs* in chicken and mice (Isaac et al. 1997; Murray and Gridley 2006) and in the chick it is also involved in the asymmetric development of the proepicardium on the right hand side (Schlueter and Brand 2009). Thus, we examined the expression pattern of *Prrx1* and *Snail1* in the chick embryo and performed functional experiments to understand the contribution of both Prrx1 and Snail1 on heart positioning.

Snail1 is also expressed in a L/R asymmetric manner in the LPM with higher levels on the right. This asymmetric expression occurs in a narrow temporal window corresponding to stages from 6 to 12 somites stage in chick embryo (Morales et al., 2007, and Figure 21A). In double-labelling experiments for *Snail1* and *Prrx1* at the 13 somite-stage we found that both were expressed asymmetrically in the *sinus venosus* horns (Figure 21B). *Prrx1* and *Snail1* display complementary expression pattern, as *Prrx1* is asymmetrically expressed in ventral splanchnic lateral mesoderm (VSPLM) and *Snail1* is asymmetrically expressed in the dorsal splanchnic lateral mesoderm (DSPLM) (Figure 22).

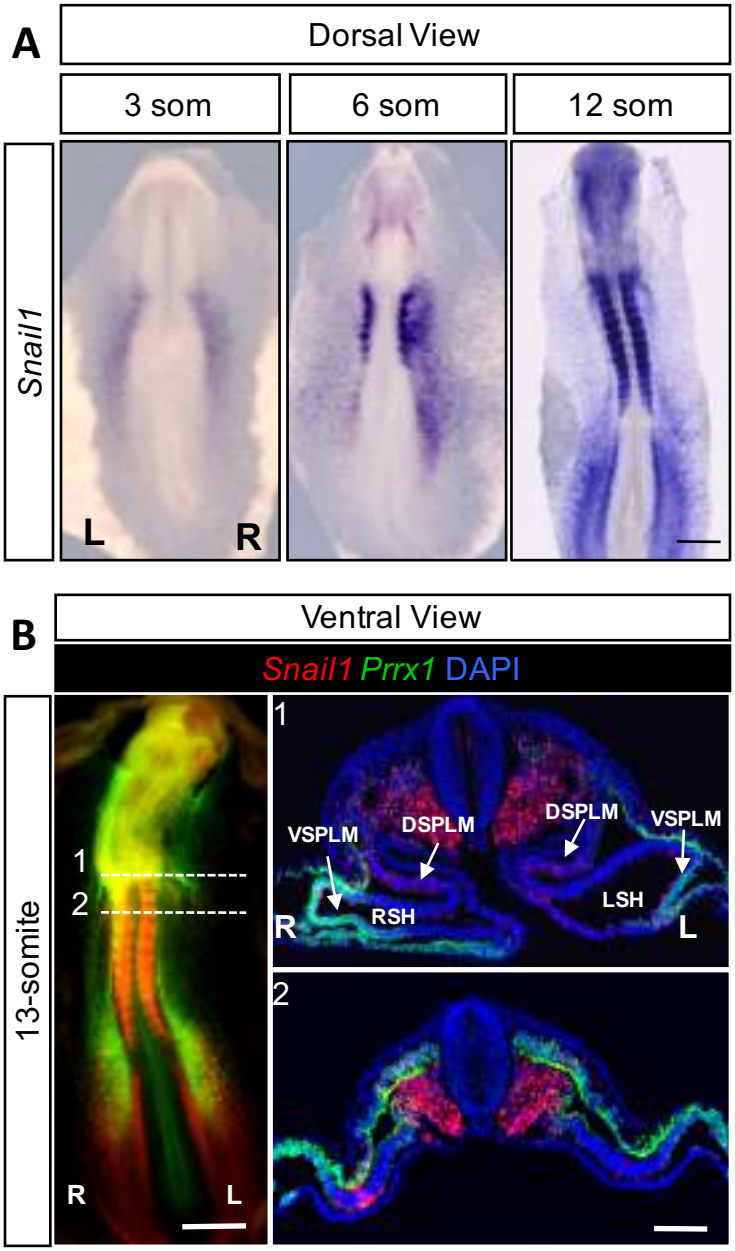

Figure 21. The asymmetric expression pattern of *Snail1* in chicken. (A) *Snail1* shows a transient asymmetric expression in the LPM of chick embryos (See also *Morales et al*., 2007). **(B)** Ventral view of whole chick embryo at 13 somite stage and transversal sections showing the transcripts for *Prrx1* and *Snail1* at the level of the *sinus venosus.* Both show complementary expression patterns in the mesodermal territories along the AP axis. DSPLM, dorsal splanchnic lateral mesoderm; VSPLM, ventral splanchnic lateral mesoderm; RSH, right *sinus venosus* horn; LSH, left *sinus venosus* horn; right *sinus venosus* horn (RSH) Scale bars, 500 µm except for the sections shown in (B), which corresponds to 100 µm.

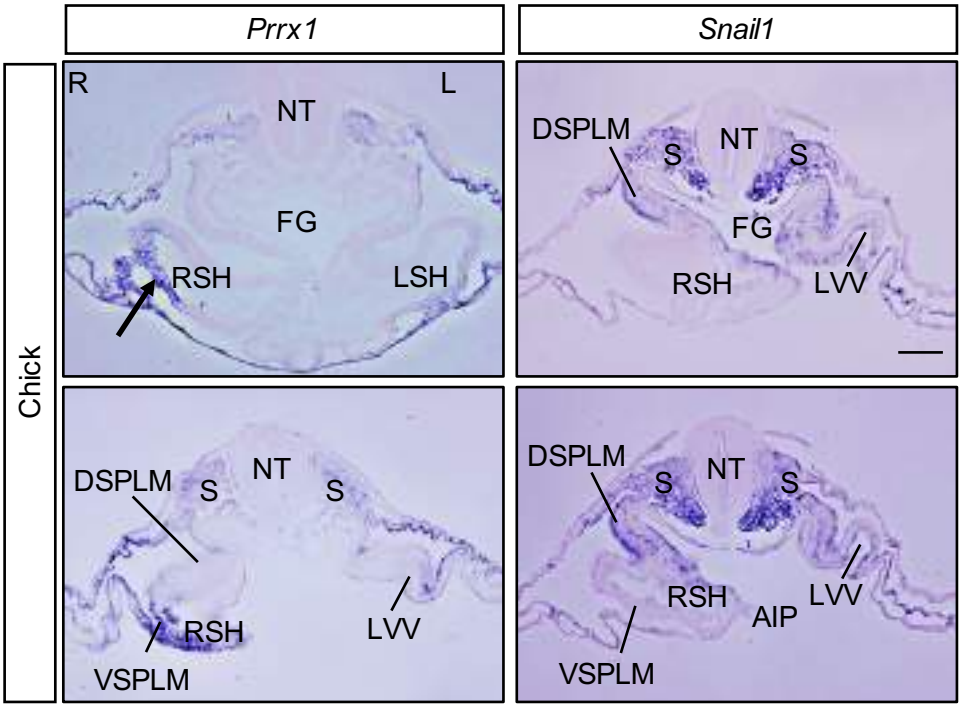

Figure 22. Complementary expression pattern of *Prrx1* and *Snail1* at the level of the *sinus venosus* in chicken embryos. *Prrx1* is asymmetrically expressed in ventral splanchnic lateral mesoderm (VSPLM) and *Snail1* is asymmetrically expressed in the dorsal splanchnic lateral mesoderm (DSPLM). Both Prrx1 and Snail1 expression is more prominent in the right *sinus venosus* horn (RSH). NT, neural tube; FG, foregut; LVV, left vitelline vein; S, somite. Scale bars, 100 μm.

We next performed loss of Snail1 function experiments by electroporating *Snail1* morpholinos (MO) (Figure 23). *Snail1* downregulation with Snail1MO reproduced the effects previously described using antisense phosphorothioated oligonucleotides (Patel et al. 1999), provoking 26,4% mesocardia and 15,7% L-loop (Figure 23A). Then, we simultaneously downregulated *Snail1* and *Prrx1* and we observed that the majority of embryos developed mesocardia (50%) and the phenotypic distribution was very similar to that found when only *Prrx1* was downregulated (Figure 23A-C). In conclusion, *Snail1* and *Prrx1* show complementary expression in the territories relevant to heart looping, but it seems that *Snail1* contributes to heart positioning acting independently from *Prrx1* and thus, that the downregulation of *Prrx1* induces mesocardia in the chick independently from Snail1 function.

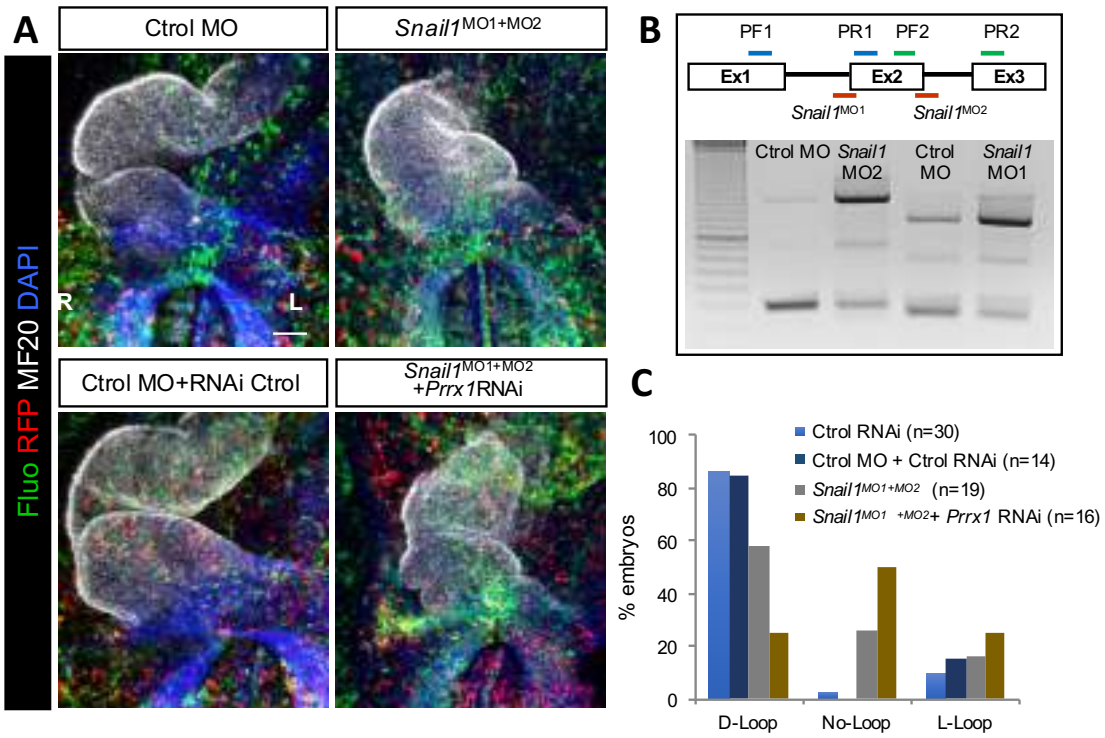

Figure 23. Snail1 contributes to heart positioning in chicken embryos. (**A**) Cardiomyocyte precursors were electroporated at stage HH3 with control fluorescein-labelled morpholinos (fluo-morpholino, Ctrol MO), with a mix of two fluo-MO against *Snail1* or with a combination of *Snail1*MOs plus *Prrx1* RNAi. In all cases an RFP construct was used as a reporter of the electroporated cells. Heart *situs* was analysed at HH11-12 by triple immunofluorescence for RFP (red), Fluorescein (green) and the cardiomyocyte marker MF20 (white). Embryos were counterstained with DAPI to visualize nuclei (blue). Panels show ventral views of maximum intensity projection of confocal images. Scale bars, 100 µm. (**B**) Schematic drawing of the *Snail1* gene and the position of the fluo-morpholinos used. Knockdown efficiency was evaluated in electroporated embryos at HH11-12 by RT-PCR amplification with primers from exon1 (PF1) and 2 (PR1) which yielded a 255 bp fragment for the mature transcript, and with primers for exon2 (PF2) and 3 (PR2) giving a PCR product of 288 bp for the mature transcript. Note the increased amount of unprocessed mRNA upon electroporation of *Snail1*MO1 and *Snail1*MO2 compared to the Control MO and the decrease of the processed transcript. (**C**) Quantitative analysis of heart *situs* in the different conditions. Ctrol MO (D-loop 86,6%, n=26; No-loop 3,3%, n=1; L-loop 10%, n=3); Ctrol MO + Ctrol RNAi (D-loop 85%, n=12; L-loop 15%, n=2); *Snail1*MO1+MO2 (D-loop 57,9%, n=11; No-loop 26,4%, n=5; L-loop 15,7%, n=3); *Snail1*MO1+MO2 + *Prrx1* RNAi (D-loop 25%, n=4; No-loop 50%, n=8; L-loop 25%, n=4).

IV.2 Heart Positioning in the Mouse

IV.2.1 Expression Patten of Prrx1 and Snail1 in The Territories Relevant to Heart Looping

Once shown that Prrx1 was involved in heart looping in both fish and chicken embryos, we wondered whether it also played a similar role in the mouse. However, we knew that the *Prrx1* or the *Prrx1/Prrx2* compound mutant mice did not show any overt heart looping defect (Bergwerff et al. 2000; Martin et al. 1995) and also that *Snail1* mutants displayed heart looping defects (Murray and Gridley 2006). Thus, we examined *Prrx1*, *Prrx2* and *Snail1* expression and compared the territories relevant to heart looping in the chick and mouse. *Snail1* was expressed in the ventral part of the *sinus venosus* horns (RSH) at higher levels on the right whereas neither *Prrx1* nor *Snail1* were expressed in the dorsal counterparts (Figure 24).

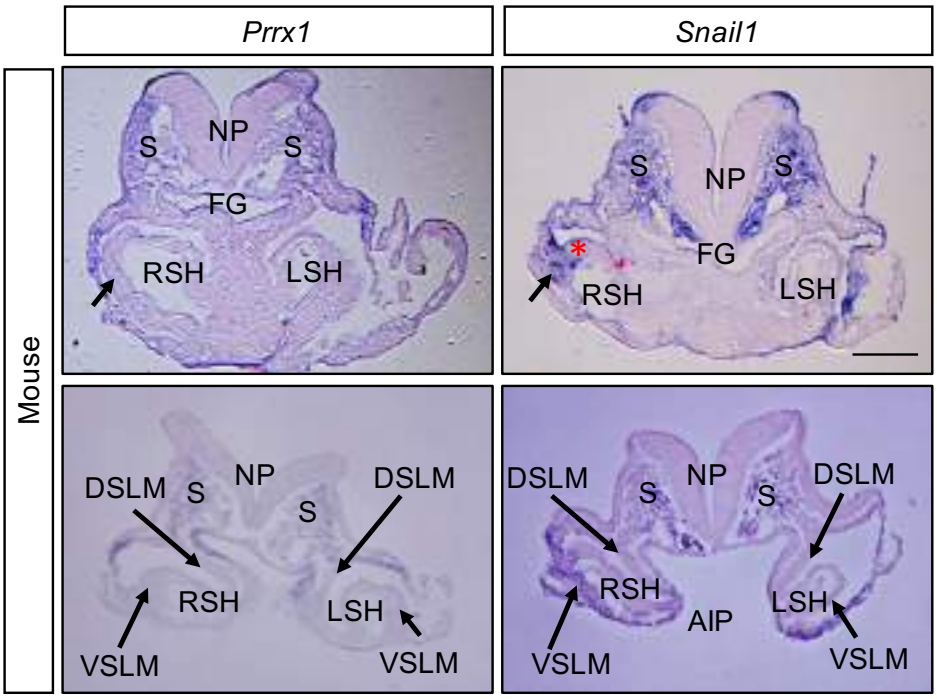

Figure 24. Comparison of *Prrx1* and *Snail1* expression at two different levels of the venous pole of the developing heart on mouse embryos (8.5 dpc). *Prrx1* is not expressed in VSLM of the embryo, where *Snail1* is expressed (arrows). *Snail1* expression is more prominent in the right *sinus venosus* horn (RSH) than the left *sinus venosus* horn (LSH). AIP, Anterior intestinal portal; FG, foregut; DSPLM, dorsal splanchnic lateral mesoderm; VSPLM, ventral splanchnic lateral mesoderm; LSH, left *sinus venosus* horn; NP, neural plate; NO, notochord; NT, neural tube; RSH, Right *sinus venosus* horn; S, somite. Scale bars, 100 μm.

Thus, the asymmetric expression of *Prrx1* in the VSPLM observed in chick embryos is replaced by that of *Snail1* in the mouse. Furthermore, we did not detect *Prrx2* expression in the territories relevant to heart looping (Figure 25). This can explain not only the absence of a heart laterality phenotype in the double *Prrx1/Prrx2* mutants (Bergwerff et al. 2000) but also the heart laterality defects observed in *Snail1* mutant mice (Murray and Gridley 2006).

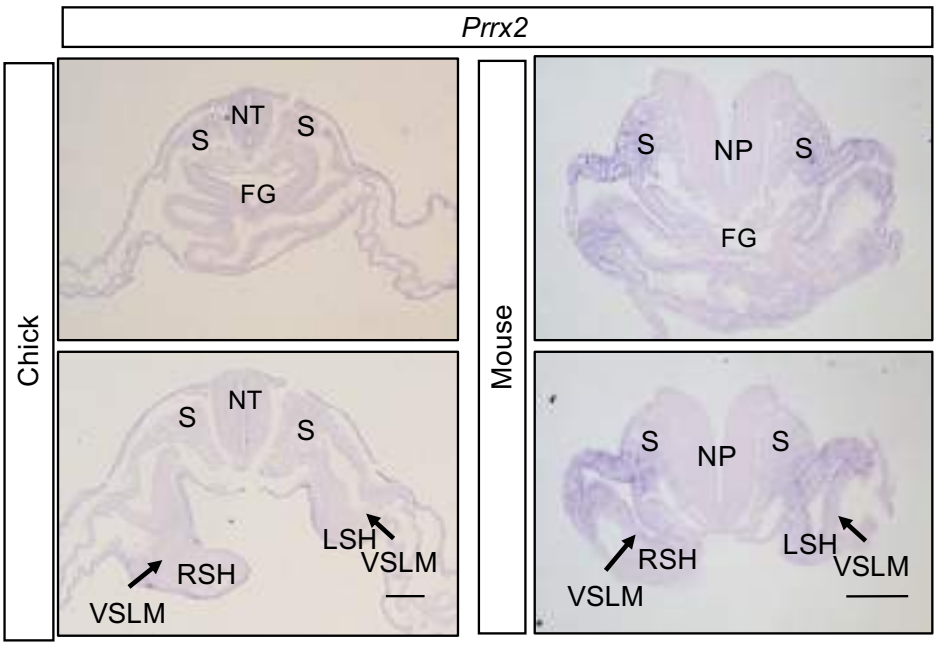

Figure 25. *Prrx2* is not expressed in the territories relevant to heart looping in chicken and mouse embryo. *Prrx2* is not expressed in VMHC, somites and foregut in chick or mouse embryos. VSPLM, ventral splanchnic lateral mesoderm; LSH, left *sinus venosus* horn; RSH, Right *sinus venosus* horn; NT, neural tube; NP, neural plate; FG, foregut; S, somite. Scale bars, 100 μm.

IV.2.2 Snail1 Downregulation Disturbs Actomyosin Mediated Differential Forces During Heart Looping

We next observed that, as in the fish and the chicken embryos, actin fibers concentrate on the right *sinus* horn, in this case coinciding with *Snail1* higher levels on the right side (Figure 26A), compatible with a similar mechanism operating to drive heart looping in the mouse, but mediated by Snail1 rather than by Prrx1. To examine whether this was indeed the case, we crossed a *Snail1* floxed allele (*Snail1*$^{fl/fl}$) with a transgenic line bearing a Tamoxifen-inducible Cre recombinase driven by the *Ubiquitin*

promoter and a ROSA26-tdTomato Cre reporter (see Methods). These mice allow controlling Snail1 depletion in a temporal manner. We left the embryo develop normally through early gastrulation stages before the addition of Tamoxifen could delete its expression. In these mice, recombinant (*Snail1* mutant) cells could be followed with tdTomato. We observed that the mutant mice displayed mesocardia (57 %) and we also performed fluorescent staining for F-actin and analyzed wt and *Snail1* mutant embryos. We observed that F-actin fibers were absent *Snail1* mutant embryos (Figure 26B) and when we analyzed *Palladin* expression we found that transcription was downregulated in the mutants (Figure 26 C).

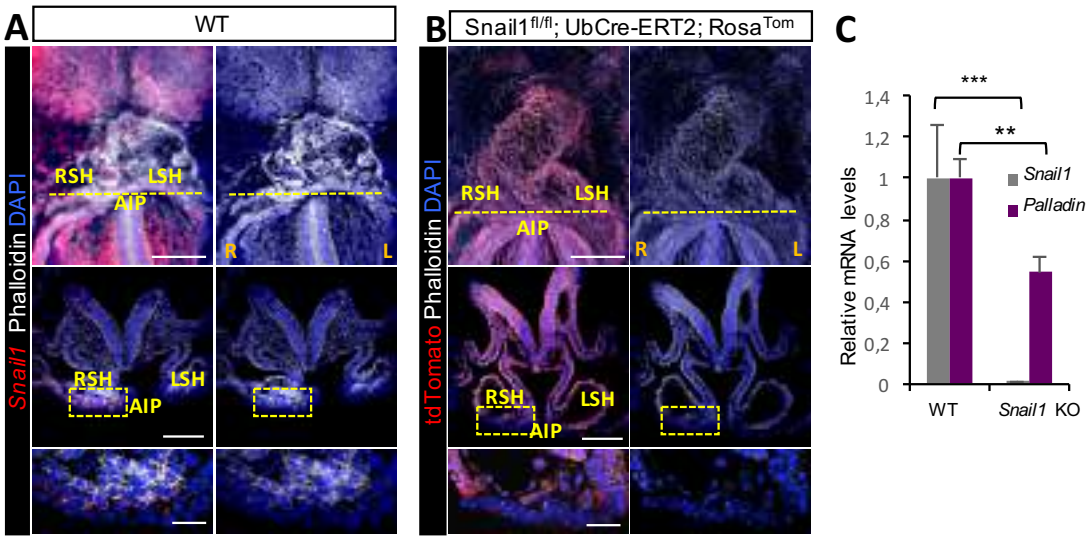

Figure 26. Asymmetric expression of *Snai1* regulates actomyosin-mediated differential forces that drive heart looping in the mouse. (A) Ventral view of an 8.5 dpc mouse embryo showing F-actin distribution revealed by phalloidin (white), which is more abundant in the right *sinus venosus* horn coinciding with *Snail1* asymmetric expression. (**B)** *Snail1* mutant cells visualized as tdTomato positive cells (red), failed to show F-actin accumulation (white). Note the L/R symmetry of the sinus horns in the mutant, compatible with the observed mesocardia. AIP, Anterior intestinal portal; LSH; left *sinus venosus* horn; RSH, Right *sinus venosus* horn (**C)** *Palladin* expression is decreased upon *Snail1* depletion. The graph shows *Snail1* and *Palladin* expression analysis of whole embryos at 8,5 dpc in a pool of 6 WT and 6 *Snail1* mutant embryos. Data represent mean ± s.e.m. ** $p<0.01$, *** $p<0.001$ by Student *t*-test. Scale bars, 100 µm except for the sections shown in (A) and (B), which correspond to 25 µm.

These data indicate that a similar cellular mechanism to that found on the fish operates in the mouse to drive heart looping and also that the molecular pathway observed downstream of Prrx1 in the fish is present in the mouse downstream of Snail1.

IV.3 The Role of Prrx1 in The Positioning of Endodermal Organs in Vertebrates

IV.3.1 Prrx1a Regulates Liver, Pancreas and Gut Position in Zebrafish

The endodermal organs are also asymmetrically positioned in the L/R axis in vertebrates. During embryonic development, the gut tube appears on the midline but subsequent looping of the intestine in the abdominal cavity results in the asymmetrical positioning of the liver, the pancreas and the gut itself.

Visceral organs are surrounded by mesoderm and the interaction between mesoderm and endoderm seems to play a crucial role on endodermal organ morphogenesis and laterality (Cayuso et al. 2016; Davis et al. 2017). As such, in zebrafish, the lateral LPM determines the chirality of gut looping and the asymmetric position of the digestive organs by undergoing specific cell movements. These movements of the LPM are cell-autonomous and under the control of L/R signalling (Horne-Badovinac et al. 2003; Yin et al. 2010). We wonder whether the mechanism that drives heart looping was also used to position the endodermal organs, or in other words, whether L/R asymmetric *Prrx1* expression in the LMP could play a role in this process. Thus, we analysed the positioning of the liver, the pancreas and the gut in control and *prrx1a* morphant embryos (similar to those analysed for heart positioning), in this case at 52 hpf stage. We used foxa3 as a global marker to visualize the developing gut tube, and the liver and pancreas buds (Field et al. 2003). Morphant embryos showed gut looping and liver and pancreas positioning defects, with the majority displaying all three organs aligned at the midline (Figure 27A). We next used the transgenic line Tg(*XlEef1a1:gut GFP*)^{s854} to visualize the gut, liver and pancreas *in vivo* (Field et al. 2003). Indeed, *prrx1a* downregulation impaired the positioning of gut, liver and pancreas (Figure 27B) and the majority (60%, 117 of 196) displayed them all aligned at the midline. In 59 of 196 morphants (30%), we observed a mirror image of the normal internal organ positioning (Figure 27C).

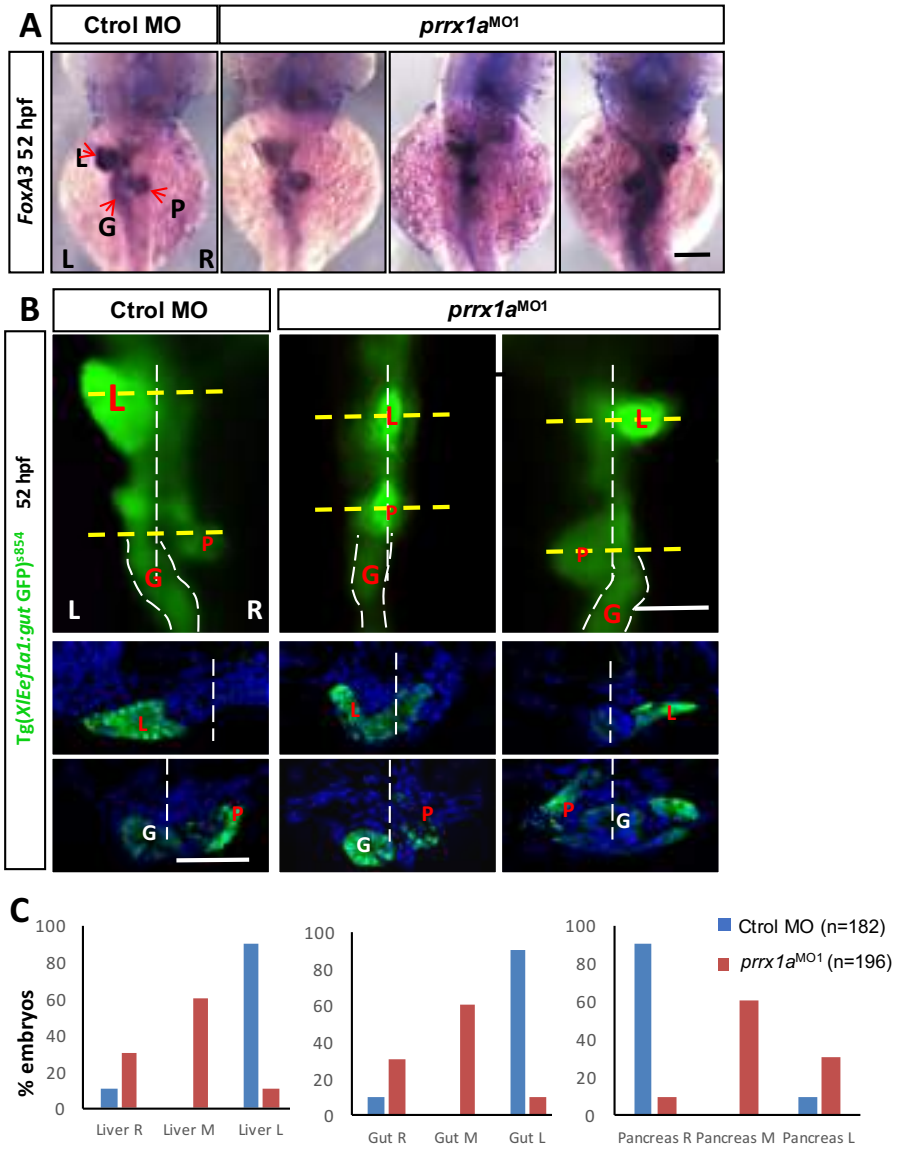

Figure 27. *Prrx1a* downregulation affects liver, pancreas and gut position in zebrafish. (**A**) Dorsal view of zebrafish embryos at 52 hpf to visualize liver, pancreas and gut position in control (Ctrol MO) and *prrx1a* morphant (*prrx1a*^{MO1}) embryos by *in situ* hybridization with a forkhead box A3 (*foxA3*) probe. (**B**) Analysis of liver, pancreas and gut *situs* in control (Ctrol MO) and *prrx1a* morphants (*prrx1a*^{MO1}) in a Tg(*XlEef1a1:gut* GFP)^{s854} reporter fish line (green) at 52 hpf. Sections correspond to liver, pancreas and gut at the level indicated by the yellow dotted lines. The white dotted lines show midline of the embryos. (**C**) Quantitative analysis of liver, pancreas and gut *situs* in control and *prrx1a* morphant embryos. Ctrol MO (Liver: Right side 10%, n=18; Midline 0%, n=0 ; L-loop 90%, n=164; Gut: Right side 10%, n=18; Midline 0%, n=0 ; L-loop 90%, n=164; Pancreas : Right side 90%, n=164; Midline 0%, n=0 ; L-loop 10%, n=18); *prrx1a*^{MO} (Liver: Right side 30%, n=59; Midline 60%, n=117 ; Left side 10%, n=20; Gut: Right side 30%, n=59; Midline 60%, n=117 ; Left side 10%, n=20; Pancreas : Right side 10%, n=20; Midline 60%, n=117 ; Left side 30%, n=59). L: Liver, G: gut, P: pancreas, R: right, M: midline, L: left. Scale bars, 100 µm.

We next wondered that how prrxa1 is linked to the asymmetric organization of the endodermal organs. As recent studies have shown that loss of Hand2 causes reduced MMP (Matrix metalloproteinases) activity at the LPM/gut boundary and blocked asymmetric LPM migration and gut looping in zebrafish (Yin et al. 2010), we examined whether *prrx1a* knockdown influenced LPM migration by assessing the position of the Hand2 positive population in a *hand2* zebrafish transgenic line Tg(*hand2:*eGFP). We analysed the LPM in *prrx1a* morphants and control embryos at 30 hpf and 52 hpf (Figure 28). We observed that downregulation of *prrx1a* impaired the migration of the LPM cells, that could not surround the gut that stays in the midline. Nevertheless, LPM cells still maintain *hand2* expression. Thus, it seems that prrx1a contributes to endodermal organ positioning, acting independently of *hand2*.

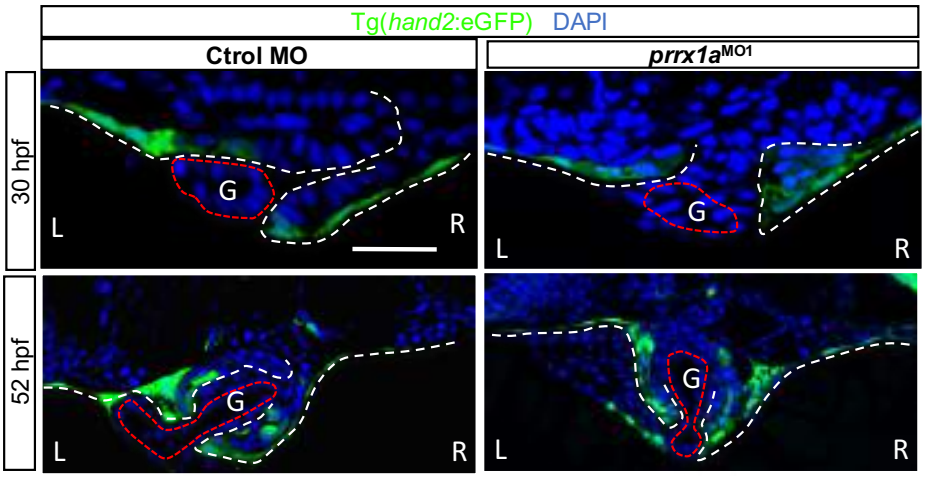

Figure 28. Defective gut-looping in zebrafish *prrx1a* morphants. Analysis of Tg(*hand2*:eGFP) expression in the LPM during gut looping in control (Ctrol MO) and *prrx1a* morphants (*prrx1a*^{MO1}) at 30 hpf and 52 hpf. The gut looped to the left in control embryos, but stayed in the midline in *prrx1a* morphants. The dashed white lines outline the right and left LPM, and the dashed red lines show the gut (G). Scale bar, 50 µm.

We then examined the expression pattern of prrx1a and compared it with that of *hand2* at different stages during zebrafish development. Prrx1 is co-expressed with *hand2* at 22 somite-stage in the LPM. Between 27 and 52 hpf stages, we detected co-expression at the most lateral part of the LMP, as we did not observe Prrx1 expression in the LPM closer to the gut (Figure 29).

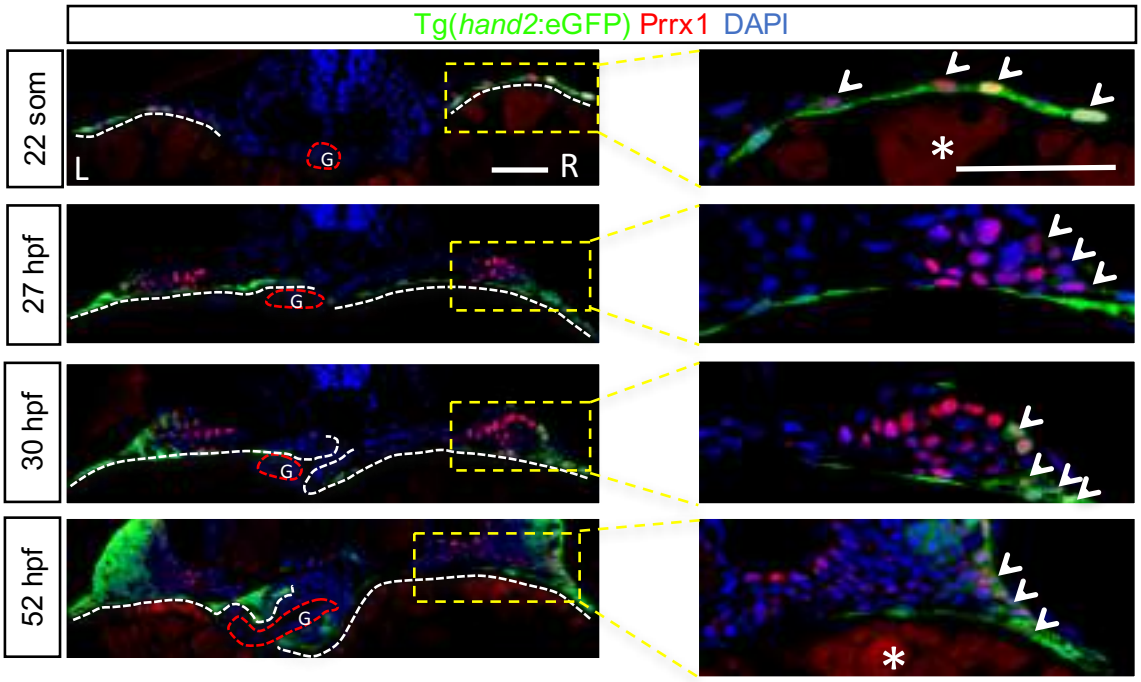

Figure 29. Time course of *Tg(hand2:*eGFP) and Prrx1 expression in the LPM during gut looping. *hand2:*GFP and Prrx1 are co-expressed on the left and the right LPM at the 22 somite stage. Between 27 and 52 hpf, there are double positive cells located at the most lateral part of LMP. Prrx1 is not expressed on the LPM close to the gut. Dashed white lines outline the right and left LPM. Sections correspond to gut (G) at the level indicated by the red dotted lines. * noise. Scale bars, 50 µm.

In summary, Prrx1 downregulation affects proper migration of the LPM and impairs gut looping and the subsequent position of liver and pancreas. Thus, asymmetric expression of Prrx1 is also sufficient for endodermal organ positioning in zebrafish.

IV.3.2 Expression Pattern of Prrx1 During Gut Looping in Chick

As the chirality of midgut looping in mammals and birds is determined by the left-right asymmetrical architecture of the dorsal mesentery (DM), a bridge of mesoderm connecting the gut tube along its entire axial length to the dorsal body wall (N. M. Davis et al. 2008; Kurpios et al. 2008), we wondered whether a similar mechanism to that observed in the fish can be also operating in other vertebrates. The asymmetrical architecture of the DM is instructed by Pitx2 and Islet1, specifically

expressed on the left side, and Tbx18, specifically expressed on the right side. Thus, we wondered whether the asymmetric expression of Prrx1 was also relevant to endodermal organ laterality in chick. Prrx1 is expressed in DM progenitor population before dorsal mesentery formation at HH17, but it is not expressed in the already looped dorsal mesentery at HH21 (Figure 30A). We also analysed *Snail1* expression in the relevant territories at very similar stages. However, we did not observe *Snail1* expression in that region (Figure 30B). Again, Prrx1 and *Snail1* seem to display complementary expression patterns. As such, Prrx1 is expressed in the DM progenitors while *Snail1* is expressed in the mesoderm that surrounds the endoderm layer (Figure 30). This expression pattern is compatible with Prrx1 playing a role in dorsal mesentery formation during gut looping. Thus, although these data are promising, we need to perform functional experiments for Prrx1 to assess whether it plays a role in gut looping in the developing chick embryo.

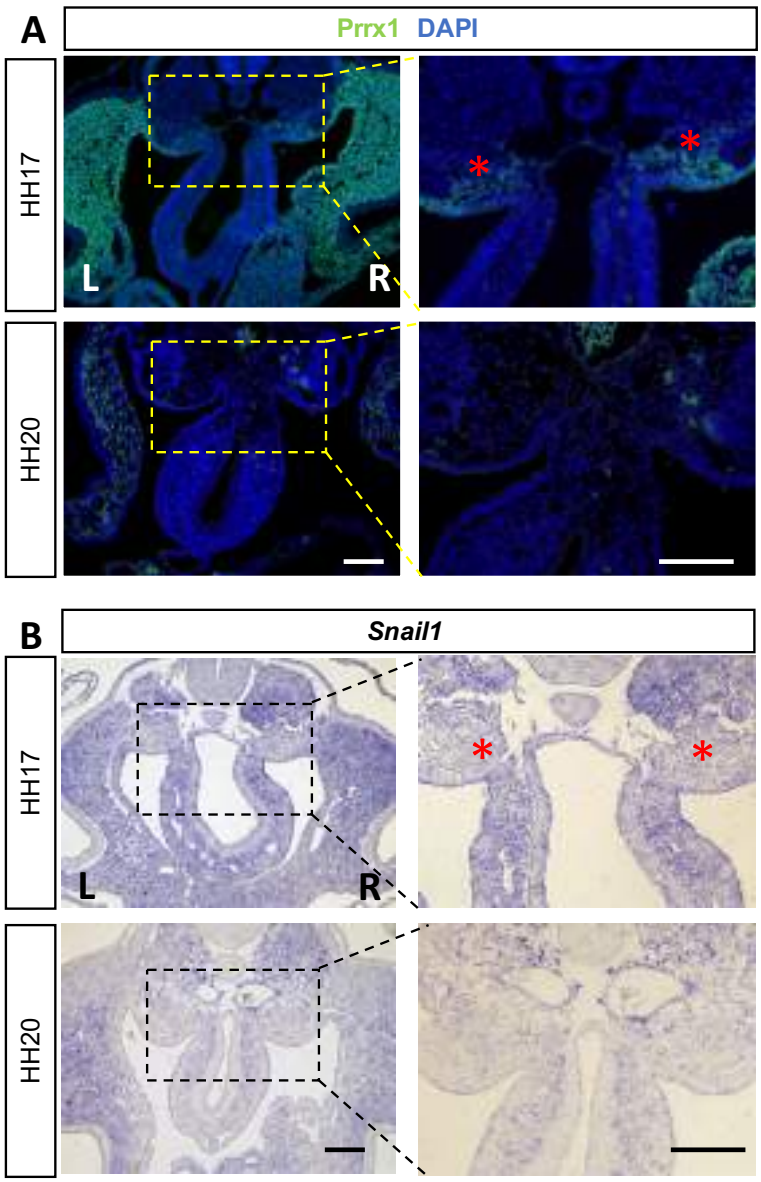

Figure 30. Analysis of Prrx1 and *Snail1* expression during dorsal mesentery development in chicken. (**A**) Prrx1 is expressed by a small population of mesodermal cells at HH17, and it is not expressed in the dorsal mesentery at HH20. Red stars, areas of Prrx1 expression. (**B**) *Snail1* is not expressed by dorsal mesentery cells. Scale bars, 100 µm.

V. DISCUSSION

The vertebrate body exhibits bilateral symmetry externally whereas the internal organs display significant left–right asymmetry. The establishment of correct left–right asymmetry is critical for survival. Thus, the mechanisms governing initiation and maintenance of these asymmetries should be tightly regulated and evolutionarily conserved. A prominent molecular cascade is driven by the Nodal-Pitx2 axis on the left-hand side of the embryo. This left-specific molecular cascade is repressed on the right-hand side by the EMT inducer, Snail in both avians and mammals (Raya and Izpisua Belmonte 2006). Recently, in the lab we have described that BMP induces the asymmetric activation of another OAR-containing transcription factor, Prrx1a, with higher levels on the right LPM. We have also shown that this L/R asymmetric expression induces a differential L/R EMT, crucial for heart looping. This indicates that not only the left side conveys instructive information and that two parallel pathways operate on the L and R to govern heart looping and morphogenesis (Ocana et al, 2017). In this work, we show that this L/R differential EMT is conserved in vertebrates as a mechanism to promote heart looping, and that a similar mechanism may also be used for the correct positioning of endodermal organs. Below, we discuss these two main conclusions in detail.

V.1 A differential L/R EMT Drives Heart Positioning in Vertebrates

The transient asymmetric distribution of Prrx1 observed in the zebrafish was also evident in the chick LPM, with higher levels on the right-hand side during a similar developmental window. Similarly, when *Prrx1* was downregulated, the embryo showed mesocardia and the size of the atrium was reduced. Thus, as in the fish, asymmetric Prrx1 expression is required for heart laterality and also for heart morphogenesis.

The cellular mechanism is also similar, as we could observe the formation of an actomyosin cable in wild type embryos, that was lost when *Prrx1* was downregulated, and compatible with the mesocardia observed. Also, as in the fish, we observed that Palladin, an actin-binding protein that promotes and maintains actin bundling in migratory and invasive cells (Gurung et al. 2016; Najm and El-Sibai 2014) was co-expressed with Prrx1, and more importantly, that it was downregulated in embryos where Prrx1 was compromised. Thus, the actomyosin-dependent leftward looping mechanism is also conserved in the chick.

Snail1 is also important for heart laterality in the chick, as downregulation of Snail1 causes a randomization of the heart *situs* (Isaac et al. 1997; Murray and Gridley 2006). Indeed, we could confirm these data after downregulation of *Snail1*, but the simultaneous downregulation of both *Prrx1* and *Snail1* did not increase the frequency of mesocardia observed when only *Prrx1* was downregulated. Given that Snail1 and Prrx1 are expressed in the splanchnic lateral mesoderm in a non-overlapping manner (dorsal and ventral parts, respectively), this indicates that Prrx1 is the main factor responsible for the mesocardia observed, as should be expected from the fact that the actomysosin cable forms in the ventral SPLM. Snail1 may still play a role in heart looping as it is possible that when the dorsal part of the SPLM is affected by the loss of Snail1, Prrx1 cannot efficiently fulfill its role even when it is expressed at normal levels. This could explain the laterality defects observed when only Snail1 is impaired. Nevertheless, further experiments analyzing the morphology of the defective Snail1 hearts is necessary to better understand its contribution to the process.

To extend our evo-devo analysis of heart looping, we examined the process in the mouse. Importantly, it was already shown that *Prrx1* mutants or *Prrx1/Prrx2* compound mutant mice do not show any overt heart looping defect (Bergwerff et al. 2000; Martin et al. 1995). We then examined the expression pattern of *Prrx1* and *Prrx2* and we found that neither *Prrx1* or its paralogue *Prrx2* were expressed in the territories relevant to heart looping. Importantly, we found that the asymmetric expression that we had observed for *Prrx1* in the VSPLM in chick embryos was replaced by that of *Snail1* in the mouse, and interestingly, that this was also a region where the F-actin fibers concentrate. Altogether, this explained (i) the absence of a heart laterality phenotype in the double *Prrx1/Prrx2* (Bergwerff et al. 2000) mutants, and (ii) the heart laterality defects observed in *Snail1* mutant mice (Murray and Gridley 2006). In fact, we could confirm that the phenotype of *Snail*1 mutant mice was mesocardia when we deleted *Snail1* at the time of heart looping in the mouse. This was very reassuring and was possible thanks to the generation of temporally conditional Snail1 mutant mouse, as conventional mutants die at gastrulation, preventing the analysis of heart looping. Again, as in the fish and chick, we could show that the mechanism depends on actomyosin and that *Palladin* transcription was downregulated in the conditional *Snail1* mutant embryos. Thus, Snail1 in the mouse seems to fulfil the role of Prrx1 in the fish and the chick in heart laterality, and the same cellular and molecular pathways that we

have observed downstream of Prrx1 in the fish and the chick, also operate in the mouse downstream of Snail1.

The differential EMT that drives heart laterality is conserved, but controlled by different transcription factors in distinct groups, Prrx1a in the zebrafish, Prrx1 and Snail1 in the chick and Snail1 in the mouse. The interchange in some expression sites of Prrx1 and Snail1 between chick and mouse is reminiscent of that observed for Snail1 and Snail2 in other migratory embryonic territories (Locascio et al. 2002). These results indicate that the use of different EMT inducers for similar processes in different species is not unique to heart laterality, and that an evolutionarily conserved role for EMT in the control of heart positioning operates from fish to mice (Figure 31 B). Thee data, together with additional experiments carried out in the lab also show that BMP induces not only Snail1 but also Prrx1 and importantly, that Pitx2 is repressed by Prrx1 in the fish. In addition, these data indicate that in the mouse, Snail1 not only represses left-handed information on the right (Murray and Gridley 2006; Patel et al. 1999) but it also instructs the right-handed pathway leading to heart looping. In the zebrafish, Prrx1a fulfils both roles. Thus, a BMP-mediated prominent right-handed pathway leads to heart laterality, and it is conserved from fish to mice although different EMT transcription factors may induce the differential L/R cell movements in different vertebrate groups (Figure 31 B, C).

In summary, while a well-described left-hand side Nodal-Pitx2 pathway promotes and stabilizes left identify (Raya and Izpisua Belmonte 2006), a BMP pathway operates prominently on the right not only to repress the Nodal-Pitx2 pathway, but also to provide instructive information that drives heart looping and morphogenesis (Figure 31 C). While the Nodal-Pitx2 axis is not conserved in worms and flies, the BMP-Prrx1 pathway activates actomyosin, and myosin has also been described as a L/R determinant in *Drosophila* (Speder et al. 2006). Hence, the effects driven by myosin would appear to play a conserved role in laterality during bilaterian evolution. Our study also indicates that an asymmetric L/R EMT process that drives differential cell movements towards the midline that are more prominent from the right, induce the leftward displacement of the posterior pole of the heart. This leftward displacement influences the direction of looping. This mechanism is conserved during evolution. Heart looping is essential for both atrio-ventricular and heart-vasculature concordance (Ramsdell 2005), and hence, for proper organ function. As such, defining the events underlying this process may shed new light on the evolution of the heart

from the simple straight invertebrate structure acting as a peristaltic pump to the suction pump found in zebrafish and to the complex rhythmically beating structure present in amniotes. Similarly, these data should help us better understand the CHDs derived from disrupted heart laterality in humans.

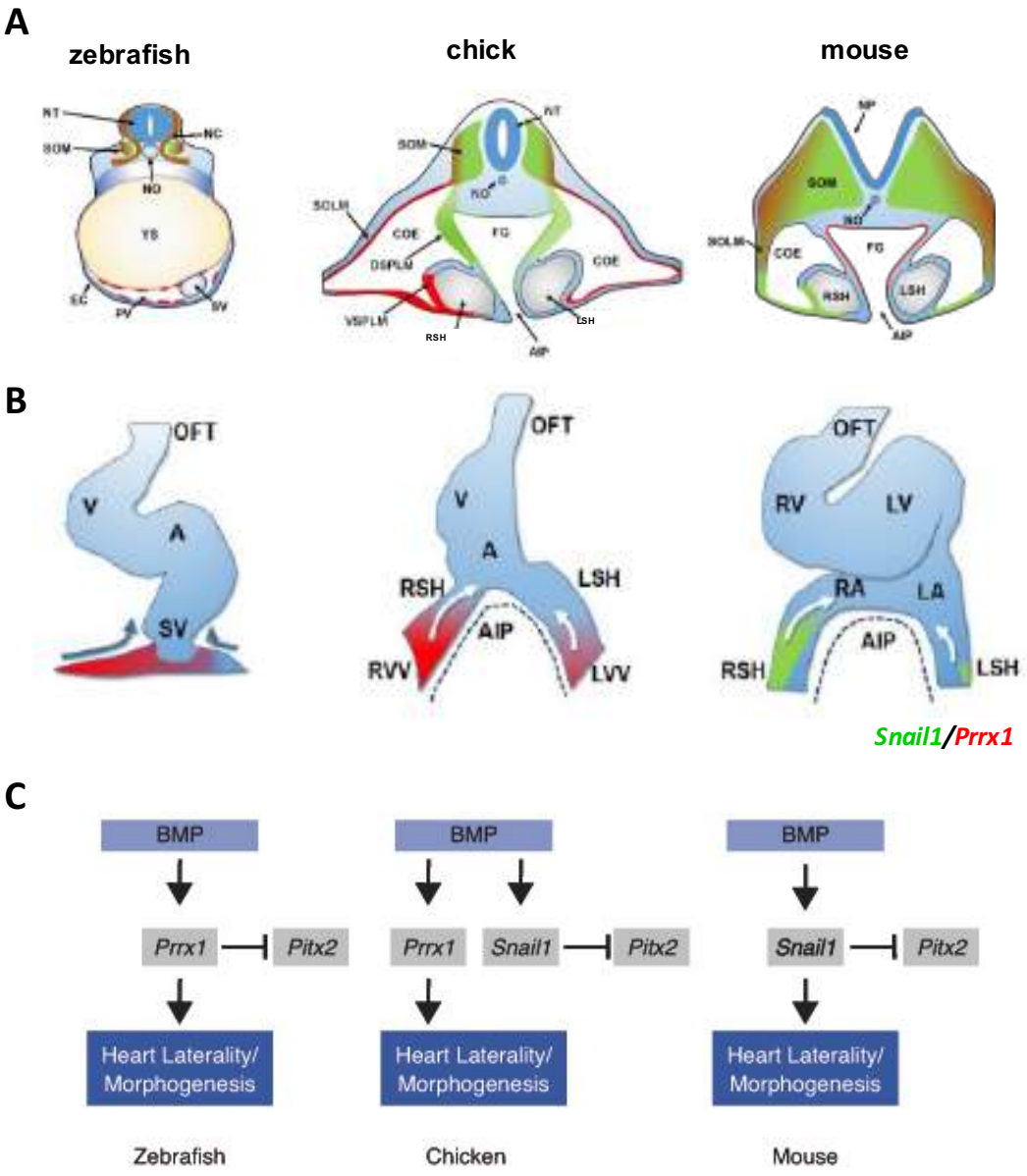

Figure 31. A differential L/R EMT drives heart positioning in vertebrates. (A) Cartoon depicting the comparative expression of *Prrx1* (red) and *Snail1* (green) in zebrafish, chick and mouse embryos. In addition, *Prrx1* is symmetrically expressed in somites (SOM) and neural crest cells (NC) in all three species. In the mouse, at an equivalent level, Prrx1 is expressed in the somatic lateral mesoderm (SOLM) and foregut endoderm (FG). The latter is another territory where *Prrx1* and *Snail1* expression is interchanged between chick and mouse. (**B**) Proposed model for heart

looping in vertebrates. In the zebrafish, the L/R asymmetric movement of Prrx1a positive cells promote a leftward position of the cardiac venous pole and the asymmetric involution (blue arrows) of the pericardium. In the chick embryonic heart there is a higher contribution of Prrx1 positive cells in the right vitelline vein (RVV), right ventral splanchnic lateral mesoderm (VSPLM) and right *sinus venosus* horn (RSH) inducing a left shift of the anterior intestinal portal (AIP) and the posterior pole of the heart (white arrows). In the mouse, Snail1 is expressed at high levels in the right *sinus venosus* horns, where it also induces a left shift of the venous pole of the heart (white arrows). AIP, Anterior intestinal portal; COE, coelom; EC, ectoderm; LSH; left *sinus venosus* horn; NP, neural plate; NO, notochord; NT, neural tube; PV, pericardial vesicle; RSH, Right *sinus venosus* horn; YS, yolk sac. (**C**) A prominent right-handed pathway drives differential L/R EMT and heart looping in vertebrates. BMP signalling activates EMT in the LPM in a L/R asymmetric manner to drive heart laterality and the exclusion of leftward information through the repression of Pitx2. This conserved cellular mechamism is implemented through the activation of different EMT inducers in different vertebrates: Prrx1a in the fish, Prrx1 and Snail1 in the chick and Snail1 in the mouse.

V.2 Prrx1 is Also Important for Positioning of Endodermal Organs in Vertebrates

The digestive system is also subjected to L/R positional cues, resulting in the asymmetrical positioning of liver, pancreas and gut with respect to the midline. The looping of the zebrafish gut results from the asymmetric migration of the neighbouring LPM and thus the asymmetric position of the digestive organs (Figure 32A). These LPM movements are cell-autonomous and the asymmetric migration of the left and right LPM is essential for leftward gut-looping morphogenesis. At the molecular level, Hand2 has been involved in this migration of the mesodermal cells that surround the gut and induce its initial leftward looping, by mainly affecting the ECM and the secretion of MMPs (Hochgreb-Hagele et al. 2013; Yin et al. 2010). Our results indicate that Prrx1a also plays an important role, as we have found that its downregulation in zebrafish affects the positioning of the endodermal organs which, in the majority of the morphant embryos, remain aligned at the midline. Indeed, we observed that after *prrx1a* downregulation the right and left LPM could not surround the gut and induce its looping. Interestingly, in contrast with the situation in the heart, the mesodermal cells influence the position but do not incorporate into the corresponding organs. This is in agreement with previous data showing that bidirectional interactions between the

mesoderm and the endoderm play a crucial role in the morphogenesis and laterality of endoderm-derived organs (Cayuso et al. 2016; A. Davis et al. 2017). However, LPM cells maintain *hand2* expression in the morphants, indicating that Prrx1 controls the asymmetrical positioning of liver, pancreas and gut in zebrafish in a Hand2-independent manner. The analysis of their expression patterns shows that *prrx1a* and *hand2* are co-expressed in the most lateral part of the LPM. However, the mesodermal cells that surround and induce the looping of the gut are *hand2* single positive. This pattern suggests that even though the *hand2*+ cells are specified independently of Prrx1a, the latter plays at least a permissive role without which *hand2* cannot fulfil its function. In other words, Prrx1 normal function is required for normal organ laterality even in the presence of Hand2.

Previous studies have assigned a role in endodermal organ asymmetry to the Nodal-Pitx2 pathway (N. M. Davis et al. 2008; Yin et al. 2010). However, in *pitx2* zebrafish mutants morphogenesis is affected, whereas L/R asymmetric looping of the gut is normal (Ji et al. 2016). Similarly, although Pitx2 overexpression affects heart laterality (reviewed in (Lopez-Gracia and Ros 2007)), *Pitx2* mouse mutants do not display heart looping defects but rather, they develop cardiac right isomerism – the absence of a left-hand side and the presence of a mirror image duplication of right-hand morphological features (Lin et al., Nature 1999; Campione et al., Dev Biol, 2001). Together with ours and previous data, it seems that Pitx2 is not involved in looping processes related to L/R asymmetries.

As we had previously addressed during the analysis of heart looping, we wondered whether this mechanism could be conserved in other vertebrates. The chirality of the midgut looping in mammals and birds is determined by the left-right asymmetrical architecture of the dorsal mesentery (DM), a bridge of mesoderm connecting the gut tube along its entire axial length to the dorsal body wall (N. M. Davis et al. 2008; Kurpios et al. 2008). Interestingly, we have found that in the chick embryo, Prrx1 is expressed by a small mesodermal cell population compatible with the precursors of the DM before gut looping and that it expression is absent in the DM after looping. As we did not detect *Snail1* expression in the relevant DM at any stage, our data are compatible with Prrx1 playing an initial role in the chirality of the midgut looping. Functional analysis of Prrx1 is required to confirm this suggestion.

In summary, our data indicate that a right-handed EMT inducer, Prrx1, drives gut looping and organizes the positioning of the pancreas and the liver in zebrafish. Thus, we propose that at least in the zebrafish, the BMP-Prrx1 mediated right-handed pathway not only controls heart laterality, but also endodermal organ laterality while Nodal-Pitx2 pathway controls morphogenesis (Figure 32 B). Further experiments are required to identify Prrx1a targets to understand the cellular and molecular mechanism by which Prrx1a drives endodermal organ looping and to confirm whether this mechanism, as we have observed for heart looping, is also conserved in vertebrates.

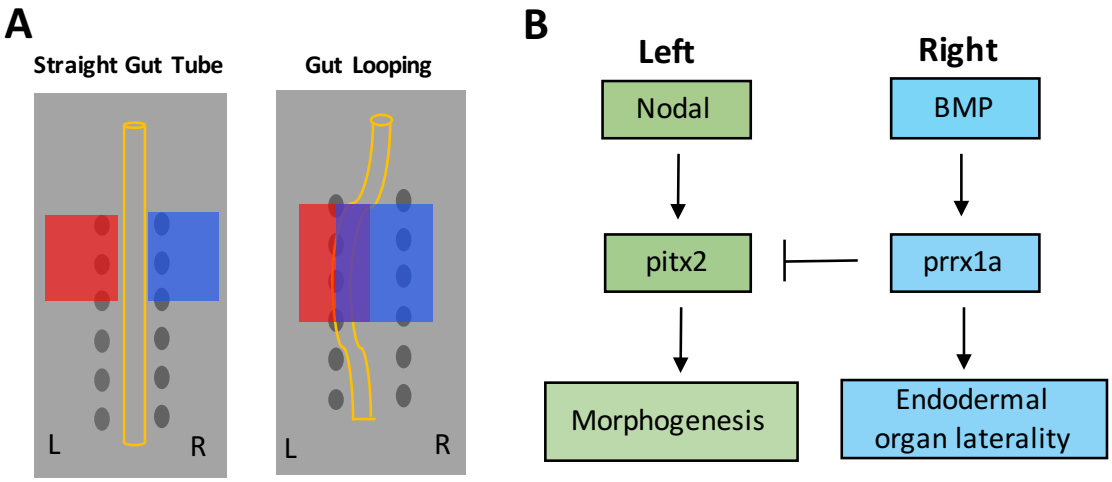

Figure 32. Prrx1 is important for endodermal organ laterality in zebrafish. (**A**) Asymmetric migration of the left and right LPM is essential for leftward gut-looping. (**B**) In the zebrafish, Prrx1 EMT inducer, drives endodermal organ laterality. BMP signalling activates Prrx1 in the LPM in a L/R asymmetric manner to drive gut laterality while Pitx2 controls organ morphogenesis. Yellow, gut tube; red, left LPM, blue, right LPM.

CONCLUSIONS

1. As in the fish, Prrx1 shows a transient L/R asymmetric expression in the chick embryo, with higher levels on the right-hand side.

2. Prrx1 also drives heart laterality in the chick through an actomyosin and Palladin-mediated mechanism.

3. Snail1 in the mouse fulfils the role of Prrx1 in the fish and chicken in heart laterality.

4. A differential L/R EMT drives heart looping in vertebrates, although the EMT-TFs vary in different species. Thus, there is an evolutionarily conserved role for EMT in the control of heart positioning.

5. Prrx1 is also important for endodermal organ positioning in zebrafish. A similar mechanism may be also operating in the chick.

VI. REFERENCES

Acloque, H., et al. (2009), 'Epithelial-mesenchymal transitions: the importance of changing cell state in development and disease', *J Clin Invest,* 119 (6), 1438-49.

Akazawa, H. and Komuro, I. (2003), 'Roles of cardiac transcription factors in cardiac hypertrophy', *Circ Res,* 92 (10), 1079-88.

Bakkers, J. (2011), 'Zebrafish as a model to study cardiac development and human cardiac disease', *Cardiovasc Res,* 91 (2), 279-88.

Barrallo-Gimeno, A. and Nieto, M. A. (2005), 'The Snail genes as inducers of cell movement and survival: implications in development and cancer', *Development,* 132 (14), 3151-61.

Bergwerff, M., et al. (2000), 'Loss of function of the Prx1 and Prx2 homeobox genes alters architecture of the great elastic arteries and ductus arteriosus', *Virchows Arch,* 436 (1), 12-9.

Blanco, M. J., et al. (2002), 'Correlation of Snail expression with histological grade and lymph node status in breast carcinomas', *Oncogene,* 21 (20), 3241-6.

Boettger, T., Wittler, L., and Kessel, M. (1999), 'FGF8 functions in the specification of the right body side of the chick', *Curr Biol,* 9 (5), 277-80.

Braasch, I., et al. (2014), 'Connectivity of vertebrate genomes: Paired-related homeobox (Prrx) genes in spotted gar, basal teleosts, and tetrapods', *Comp Biochem Physiol C Toxicol Pharmacol,* 163, 24-36.

Branford, W. W. and Yost, H. J. (2004), 'Nodal signaling: CrypticLefty mechanism of antagonism decoded', *Curr Biol,* 14 (9), R341-3.

Brennan, J., et al. (2001), 'Nodal signalling in the epiblast patterns the early mouse embryo', *Nature,* 411 (6840), 965-9.

Bressan, M., Liu, G., and Mikawa, T. (2013), 'Early mesodermal cues assign avian cardiac pacemaker fate potential in a tertiary heart field', *Science,* 340 (6133), 744-8.

Campione, M., et al. (1999), 'The homeobox gene Pitx2: mediator of asymmetric left-right signaling in vertebrate heart and gut looping', *Development,* 126 (6), 1225-34.

Cano, A., et al. (2000), 'The transcription factor snail controls epithelial-mesenchymal transitions by repressing E-cadherin expression', *Nat Cell Biol,* 2 (2), 76-83.

Cano, E., et al. (2016), 'Extracardiac septum transversum/proepicardial endothelial cells pattern embryonic coronary arterio-venous connections', *Proc Natl Acad Sci U S A,* 113 (3), 656-61.

Carver, E. A., et al. (2001), 'The mouse snail gene encodes a key regulator of the epithelial-mesenchymal transition', *Mol Cell Biol,* 21 (23), 8184-8.

Cayuso, J., et al. (2016), 'EphrinB1/EphB3b Coordinate Bidirectional Epithelial-Mesenchymal Interactions Controlling Liver Morphogenesis and Laterality', *Dev Cell,* 39 (3), 316-28.

Chea, H. K., Wright, C. V., and Swalla, B. J. (2005), 'Nodal signaling and the evolution of deuterostome gastrulation', *Dev Dyn,* 234 (2), 269-78.

Come, C., et al. (2006), 'Snail and slug play distinct roles during breast carcinoma progression', *Clin Cancer Res,* 12 (18), 5395-402.

Cserjesi, P., et al. (1992), 'MHox: a mesodermally restricted homeodomain protein that binds an essential site in the muscle creatine kinase enhancer', *Development,* 115 (4), 1087-101.

Davidson, B. P. and Tam, P. P. (2000), 'The node of the mouse embryo', *Curr Biol,* 10 (17), R617-9.

Davis, A., et al. (2017), 'Stomach curvature is generated by left-right asymmetric gut morphogenesis', *Development,* 144 (8), 1477-83.

Davis, N. M., et al. (2008), 'The chirality of gut rotation derives from left-right asymmetric changes in the architecture of the dorsal mesentery', *Dev Cell,* 15 (1), 134-45.

Dominguez, J. N., et al. (2012), 'Asymmetric fate of the posterior part of the second heart field results in unexpected left/right contributions to both poles of the heart', *Circ Res,* 111 (10), 1323-35.

Dougan, S. T., et al. (2003), 'The role of the zebrafish nodal-related genes squint and cyclops in patterning of mesendoderm', *Development,* 130 (9), 1837-51.

Essner, J. J., et al. (2000), 'Mesendoderm and left-right brain, heart and gut development are differentially regulated by pitx2 isoforms', *Development,* 127 (5), 1081-93.

Essner, J. J., et al. (2005), 'Kupffer's vesicle is a ciliated organ of asymmetry in the zebrafish embryo that initiates left-right development of the brain, heart and gut', *Development,* 132 (6), 1247-60.

Field, H. A., et al. (2003), 'Formation of the digestive system in zebrafish. I. Liver morphogenesis', *Dev Biol,* 253 (2), 279-90.

Galliot, B., de Vargas, C., and Miller, D. (1999), 'Evolution of homeobox genes: Q50 Paired-like genes founded the Paired class', *Dev Genes Evol,* 209 (3), 186-97.

Grande, M. T., et al. (2015), 'Snail1-induced partial epithelial-to-mesenchymal transition drives renal fibrosis in mice and can be targeted to reverse established disease', *Nat Med,* 21 (9), 989-97.

Gurung, R., et al. (2016), 'Actin polymerization is stimulated by actin cross-linking protein palladin', *Biochem J,* 473 (4), 383-96.

Hamburger, V. and Hamilton, H. L. (1992), 'A series of normal stages in the development of the chick embryo. 1951', *Dev Dyn,* 195 (4), 231-72.

Hami, D., et al. (2011), 'Zebrafish cardiac development requires a conserved secondary heart field', *Development,* 138 (11), 2389-98.

Hernandez-Torres, F., et al. (2017), 'Pitx2 in Embryonic and Adult Myogenesis', *Front Cell Dev Biol,* 5, 46.

Hernandez-Vega, A. and Minguillon, C. (2011), 'The Prx1 limb enhancers: targeted gene expression in developing zebrafish pectoral fins', *Dev Dyn,* 240 (8), 1977-88.

Hirokawa, N., Tanaka, Y., and Okada, Y. (2009), 'Left-right determination: involvement of molecular motor KIF3, cilia, and nodal flow', *Cold Spring Harb Perspect Biol,* 1 (1), a000802.

Hirokawa, N., et al. (2006), 'Nodal flow and the generation of left-right asymmetry', *Cell,* 125 (1), 33-45.

Hochgreb-Hagele, T., et al. (2013), 'Laminin beta1a controls distinct steps during the establishment of digestive organ laterality', *Development,* 140 (13), 2734-45.

Horne-Badovinac, S., Rebagliati, M., and Stainier, D. Y. (2003), 'A cellular framework for gut-looping morphogenesis in zebrafish', *Science,* 302 (5645), 662-5.

Icardo, J. M., Garcia Rincon, J. M., and Ros, M. A. (2002), '[Congenital heart disease, heterotaxia and laterality]', *Rev Esp Cardiol,* 55 (9), 962-74.

Isaac, A., Sargent, M. G., and Cooke, J. (1997), 'Control of vertebrate left-right asymmetry by a snail-related zinc finger gene', *Science,* 275 (5304), 1301-4.

Ji, Y., Buel, S. M., and Amack, J. D. (2016), 'Mutations in zebrafish pitx2 model congenital malformations in Axenfeld-Rieger syndrome but do not disrupt left-right placement of visceral organs', *Dev Biol,* 416 (1), 69-81.

Kalluri, R. and Weinberg, R. A. (2009), 'The basics of epithelial-mesenchymal transition', *J Clin Invest,* 119 (6), 1420-8.

Kawasumi, A., et al. (2011), 'Left-right asymmetry in the level of active Nodal protein produced in the node is translated into left-right asymmetry in the lateral plate of mouse embryos', *Dev Biol,* 353 (2), 321-30.

Kestens, C., et al. (2016), 'BMP4 Signaling Is Able to Induce an Epithelial-Mesenchymal Transition-Like Phenotype in Barrett's Esophagus and Esophageal Adenocarcinoma through Induction of SNAIL2', *PLoS One,* 11 (5), e0155754.

Kimmel, C. B., et al. (1995), 'Stages of embryonic development of the zebrafish', *Dev Dyn,* 203 (3), 253-310.

Krainock, M., et al. (2016), 'Epicardial Epithelial-to-Mesenchymal Transition in Heart Development and Disease', *J Clin Med,* 5 (2).

Kurpios, N. A., et al. (2008), 'The direction of gut looping is established by changes in the extracellular matrix and in cell:cell adhesion', *Proc Natl Acad Sci U S A,* 105 (25), 8499-506.

Levin, M., et al. (1995), 'A molecular pathway determining left-right asymmetry in chick embryogenesis', *Cell,* 82 (5), 803-14.

Lin, A. E., et al. (2014), 'Laterality defects in the national birth defects prevention study (1998-2007): birth prevalence and descriptive epidemiology', *Am J Med Genet A,* 164A (10), 2581-91.

Lin, C. R., et al. (1999), 'Pitx2 regulates lung asymmetry, cardiac positioning and pituitary and tooth morphogenesis', *Nature,* 401 (6750), 279-82.

Locascio, A., et al. (2002), 'Modularity and reshuffling of Snail and Slug expression during vertebrate evolution', *Proc Natl Acad Sci U S A,* 99 (26), 16841-6.

Logan, M., et al. (1998), 'The transcription factor Pitx2 mediates situs-specific morphogenesis in response to left-right asymmetric signals', *Cell,* 94 (3), 307-17.

Lopez-Gracia, M. L. and Ros, M. A. (2007), 'Left-right asymmetry in vertebrate development', *Adv Anat Embryol Cell Biol,* 188, 1-121, back cover.

Lovisa, S., et al. (2015), 'Epithelial-to-mesenchymal transition induces cell cycle arrest and parenchymal damage in renal fibrosis', *Nat Med,* 21 (9), 998-1009.

Madisen, L., et al. (2010), 'A robust and high-throughput Cre reporting and characterization system for the whole mouse brain', *Nat Neurosci,* 13 (1), 133-40.

Martin, J. F., Bradley, A., and Olson, E. N. (1995), 'The paired-like homeo box gene MHox is required for early events of skeletogenesis in multiple lineages', *Genes Dev,* 9 (10), 1237-49.

Monsoro-Burq, A. and Le Douarin, N. M. (2001), 'BMP4 plays a key role in left-right patterning in chick embryos by maintaining Sonic Hedgehog asymmetry', *Mol Cell,* 7 (4), 789-99.

Morales, A. V., et al. (2007), 'Snail genes at the crossroads of symmetric and asymmetric processes in the developing mesoderm', *EMBO Rep,* 8 (1), 104-9.

Mucchielli, M. L., et al. (1997), 'Mouse Otlx2/RIEG expression in the odontogenic epithelium precedes tooth initiation and requires mesenchyme-derived signals for its maintenance', *Dev Biol,* 189 (2), 275-84.

Murray, S. A. and Gridley, T. (2006), 'Snail family genes are required for left-right asymmetry determination, but not neural crest formation, in mice', *Proc Natl Acad Sci U S A,* 103 (27), 10300-4.

Najm, P. and El-Sibai, M. (2014), 'Palladin regulation of the actin structures needed for cancer invasion', *Cell Adh Migr,* 8 (1), 29-35.

Nasevicius, A. and Ekker, S. C. (2001), 'The zebrafish as a novel system for functional genomics and therapeutic development applications', *Curr Opin Mol Ther,* 3 (3), 224-8.

Nieto, M. A., et al. (2016), 'Emt: 2016', *Cell,* 166 (1), 21-45.

Nohno, T., et al. (1993), 'A chicken homeobox gene related to Drosophila paired is predominantly expressed in the developing limb', *Dev Biol,* 158 (1), 254-64.

Norris, R. A. and Kern, M. J. (2001), 'The identification of Prx1 transcription regulatory domains provides a mechanism for unequal compensation by the Prx1 and Prx2 loci', *J Biol Chem,* 276 (29), 26829-37.

Ocana, O. H., et al. (2017), 'A right-handed signalling pathway drives heart looping in vertebrates', *Nature,* 21.

Ocana, O. H., et al. (2012), 'Metastatic colonization requires the repression of the epithelial-mesenchymal transition inducer Prrx1', *Cancer Cell,* 22 (6), 709-24.

Okada, Y., et al. (2005), 'Mechanism of nodal flow: a conserved symmetry breaking event in left-right axis determination', *Cell,* 121 (4), 633-44.

Patel, K., Isaac, A., and Cooke, J. (1999), 'Nodal signalling and the roles of the transcription factors SnR and Pitx2 in vertebrate left-right asymmetry', *Curr Biol,* 9 (11), 609-12.

Ploski, J. E., Shamsher, M. K., and Radu, A. (2004), 'Paired-type homeodomain transcription factors are imported into the nucleus by karyopherin 13', *Mol Cell Biol,* 24 (11), 4824-34.

Ramsdell, A. F. (2005), 'Left-right asymmetry and congenital cardiac defects: getting to the heart of the matter in vertebrate left-right axis determination', *Dev Biol,* 288 (1), 1-20.

Ramsdell, A. F. and Yost, H. J. (1999), 'Cardiac looping and the vertebrate left-right axis: antagonism of left-sided Vg1 activity by a right-sided ALK2-dependent BMP pathway', *Development,* 126 (23), 5195-205.

Rana, M. S., et al. (2014), 'Tbx1 coordinates addition of posterior second heart field progenitor cells to the arterial and venous poles of the heart', *Circ Res,* 115 (9), 790-9.

Raya, A. and Izpisua Belmonte, J. C. (2006), 'Left-right asymmetry in the vertebrate embryo: from early information to higher-level integration', *Nat Rev Genet,* 7 (4), 283-93.

Reichert, M., et al. (2013), 'The Prrx1 homeodomain transcription factor plays a central role in pancreatic regeneration and carcinogenesis', *Genes Dev,* 27 (3), 288-300.

Rowe, R. G., et al. (2009), 'Mesenchymal cells reactivate Snail1 expression to drive three-dimensional invasion programs', *J Cell Biol,* 184 (3), 399-408.

Ruzankina, Y., et al. (2007), 'Deletion of the developmentally essential gene ATR in adult mice leads to age-related phenotypes and stem cell loss', *Cell Stem Cell,* 1 (1), 113-26.

Ryan, A. K., et al. (1998), 'Pitx2 determines left-right asymmetry of internal organs in vertebrates', *Nature,* 394 (6693), 545-51.

Schlueter, J. and Brand, T. (2009), 'A right-sided pathway involving FGF8/Snai1 controls asymmetric development of the proepicardium in the chick embryo', *Proc Natl Acad Sci U S A,* 106 (18), 7485-90.

Schweickert, A., et al. (2000), 'Pitx2 isoforms: involvement of Pitx2c but not Pitx2a or Pitx2b in vertebrate left-right asymmetry', *Mech Dev,* 90 (1), 41-51.

Sefton, M., Sanchez, S., and Nieto, M. A. (1998), 'Conserved and divergent roles for members of the Snail family of transcription factors in the chick and mouse embryo', *Development,* 125 (16), 3111-21.

Semina, E. V., Reiter, R. S., and Murray, J. C. (1997), 'Isolation of a new homeobox gene belonging to the Pitx/Rieg family: expression during lens development and mapping to the aphakia region on mouse chromosome 19', *Hum Mol Genet,* 6 (12), 2109-16.

Semina, E. V., et al. (1996), 'Cloning and characterization of a novel bicoid-related homeobox transcription factor gene, RIEG, involved in Rieger syndrome', *Nat Genet,* 14 (4), 392-9.

Shen, M. M. (2007), 'Nodal signaling: developmental roles and regulation', *Development,* 134 (6), 1023-34.

Shimozaki, K., Clemenson, G. D., Jr., and Gage, F. H. (2013), 'Paired related homeobox protein 1 is a regulator of stemness in adult neural stem/progenitor cells', *J Neurosci,* 33 (9), 4066-75.

Smith, K. A., et al. (2011), 'Bmp and nodal independently regulate lefty1 expression to maintain unilateral nodal activity during left-right axis specification in zebrafish', *PLoS Genet,* 7 (9), e1002289.

Soukup, V., et al. (2015), 'The Nodal signaling pathway controls left-right asymmetric development in amphioxus', *Evodevo,* 6, 5.

Speder, P., Adam, G., and Noselli, S. (2006), 'Type ID unconventional myosin controls left-right asymmetry in Drosophila', *Nature,* 440 (7085), 803-7.

Speder, P., et al. (2007), 'Strategies to establish left/right asymmetry in vertebrates and invertebrates', *Curr Opin Genet Dev,* 17 (4), 351-8.

Theriault, B. L., et al. (2007), 'BMP4 induces EMT and Rho GTPase activation in human ovarian cancer cells', *Carcinogenesis,* 28 (6), 1153-62.

Thiery, J. P., et al. (2009), 'Epithelial-mesenchymal transitions in development and disease', *Cell,* 139 (5), 871-90.

von Gise, A. and Pu, W. T. (2012), 'Endocardial and epicardial epithelial to mesenchymal transitions in heart development and disease', *Circ Res,* 110 (12), 1628-45.

Wang, R. N., et al. (2014), 'Bone Morphogenetic Protein (BMP) signaling in development and human diseases', *Genes Dis,* 1 (1), 87-105.

Welsh, I. C., et al. (2013), 'Integration of left-right Pitx2 transcription and Wnt signaling drives asymmetric gut morphogenesis via Daam2', *Dev Cell,* 26 (6), 629-44.

Wright, C. V. (2001), 'Mechanisms of left-right asymmetry: what's right and what's left?', *Dev Cell,* 1 (2), 179-86.

Xie, L., et al. (2012), 'Tbx5-hedgehog molecular networks are essential in the second heart field for atrial septation', *Dev Cell,* 23 (2), 280-91.

Yin, C., et al. (2010), 'Hand2 regulates extracellular matrix remodeling essential for gut-looping morphogenesis in zebrafish', *Dev Cell,* 18 (6), 973-84.

Yu, X., et al. (2001), 'Differential expression and functional analysis of Pitx2 isoforms in regulation of heart looping in the chick', *Development,* 128 (6), 1005-13.